Chapter 6

Objective 3

Amphiphilic Hyaluronic acid and Chitosan-based Nanoparticles incorporated in Dissolving Microneedles for Localized Delivery of Cabazitaxel

6 Hyaluronic acid-oleylamine and chitosan-oleic acid conjugate-based hybrid nanoparticle delivery via. dissolving microneedles for enhanced treatment efficacy in localized breast cancer

6.1 Introduction

Microneedles are a promising technology for transdermal drug delivery owing to their capability to penetrate the biological barrier of stratum corneum and thus delivering the therapeutic agents directly into the underlying tissues [215,216]. In the context of breast cancer treatment, researchers have been exploring the use of microneedles to deliver drugs that target tumors more effectively while minimizing systemic side effects [217]. Traditional routes of drug administration, such as oral intake or intravenous injection, may not always provide optimal drug delivery to breast tumors [218,219]. The non-selective systemic administration of chemotherapeutics causes off-site distribution, leading to systemic toxicity and potential higher dose requirements. Microneedles offer a minimally invasive approach that can bypass the skin barrier and deliver drugs directly to the tumor site, enhancing drug concentration and therapeutic efficacy while reducing systemic toxicity [220,221]. Additionally, microneedles also address the challenges of patient compliance in chemotherapeutic regime due to its ease of administration, as it doesn't require any skilled supervision [222,223].

Drugs for breast cancer treatment, such as chemotherapy agents, proteins, peptides, genes, antibodies or vaccine can be loaded onto or encapsulated within microneedles [224,225]. Also, the ineffectiveness of conventional therapies is often the result of therapeutic resistance [226,227]. Loading the chemotherapeutics in nanosized carriers has been shown to improve the drug efficacy and overcome the resistance [150,228,229]. Additionally, surface modifications or functionalization of the nanoparticles using ligands or antibodies targeting overexpressed receptors on breast cancer cells can facilitate active targeting [230].

Present study employed integration of aforementioned approaches to develop an advanced drug delivery system of dissolving microneedle loaded with cetuximab (Cmab) functionalized hyaluronic acid-oleylamine (HA-OA) and chitosan-oleic acid (CS-OA) conjugate-based hybrid nanoparticles loaded with Cabazitaxel (CBT) for targeted and localized breast cancer therapy. Natural biopolymers such as Chitosan and Hyaluronic acid have been used here due their opposite charge, biocompatibility, and ease of modification on the backbone of these polysaccharides allowing for the preparation of functionalized nanosystems. The anionic nature of hyaluronic acid complements the cationic nature of chitosan in forming particles via. ionic gelation. Conjugating these polysaccharides with a hydrophobic moiety renders them amphiphilic and allows for the formation of a micellar structure that subsequently forms a particle due to electrostatic interaction between the anionic carboxylic acid of hyaluronic acid and amine of chitosan (ionic gelation). Also, the amphiphilic derivatives of these hydrophilic polymers have been reported to show better encapsulation of hydrophobic drugs and superior intracellular delivery of therapeutic payload. The incorporation of TPGS in the nanoparticles further improves the stability of the nanoparticles and reduces the size of the formed system. TPGS also been reported to prevent the P-gp-mediated efflux of the nanoparticles from the cell.

The dissolving microneedle was prepared using polymeric blend of high molecular weight hyaluronic acid (HA), Polyvinyl Alcohol (PVA), and Polyvinyl Pyrrolidine (PVP) [221,231]. The biodegradability of these polymers allows for multiple microneedle applications in a treatment regimen [232]. The hydrophilicity of HA and PVA, along with super disintegrant PVP, provides a perfect blend of polymers that can interact with the aqueous media and dissolve immediately. Besides, HA/PVA/PVP blends has been previously reported for the fabrication of dissolvable microneedles[233].

We hypothesize, that the dissolving microneedle array can create microchannels in the rat skin on application over solid tumor and readily dissolve upon exposure to the water in skin [234,235]. The polymeric matrix would act as a depot for the nanoparticles loaded in the polymeric blend, allowing site-specific delivery of loaded HA-OA/CS-OA NPT in solid localized tumors. The microchannels can also be utilized by the nanoparticles in the backing layer to reach target site. The HA-OA/CS-OA NPT with particle size <130 nm at tumor site can offer selective intracellular accumulation of loaded CBT due to EGFR-mediated endocytosis in breast cancer. Therefore, these fabricated microneedles loaded with targeted nanoparticles may provide a viable treatment alternative for targeted and localized breast cancer therapy with superior efficacy than the conventional intravenous regimen.

6.2 Materials and methods

6.2.1 Materials required

Cabazitaxel (CBT) was received as a gift sample from Hetero Labs, India. Sodium Hyaluronate, average molecular weight ~7.6 kDa and High molecular weight Sodium Hyaluronate (HA), average molecular weight ~38 kDa was obtained as a gift sample by Shandong Topscience Biotech Co. Ltd., Shandong, PRC. D-alpha-Tocopheryl polyethylene glycol 1000 succinate (TPGS) was gift sample from Antares Health Products, St. Charles, USA. Chitosan (CS), Succinic anhydride (SA), Oleylamine, oleic acid N, N-Dimethylpyridin-4-amine (DMAP), and 1-(3-Dimethylaminopropyl)-3-ethylcarbodiimide hydrochloride (EDC) were procured from SRL Pvt. Ltd. N-hydroxysulfosuccinimide (Sulfo-NHS) was procured from TCI (India) Pvt. Ltd. All the other chemicals and solvents used in the experiments were of high purity grade.

MDA-MB-231 (breast cancer adenocarcinoma) were sourced from NCCS in Pune, India. We obtained DMEM (Dulbecco's Modified Eagle Medium) and 12-well cell culture plate

from Genetix Pvt. Ltd. Additionally, we acquired 96-well plates and T-25 flasks were obtained from Eppendorf. Penicillin-streptomycin, Trypsin-EDTA, and FBS (Fetal Bovine Serum) were purchased from Gibco. We prepared Phosphate Buffer Saline (PBS) using a reliable analytical chemical.

6.2.2 Synthesis of CS-OA, HA-OA, and TPGS-COOH

Figure 6.1 provides the schematic representation of Hyaluronic acid–oleylamine conjugate (HA-OA), Chitosan–oleic acid conjugate (CS-OA), and Succinylated TPGS (TPGS-COOH) conjugate synthesis, used for the formulation of nanoparticles. The hyaluronic acid-oleylamine conjugate was synthesized using carbodiimide chemistry [236]. Briefly, 1165 mg of Hyaluronic acid was dissolved in 20 mL of 0.1 M MES buffered saline pH 5.5 containing 210 mg of EDAC HCl and 140 mg of NHS. The solution was stirred for 1 hour to ensure the activation of carboxylic acid in the hyaluronic acid backbone. Subsequently, 470 µl of 70% oleylamine diluted with 4.53 mL of ethanol was added dropwise into the hyaluronic acid solution. The reaction mixture was allowed to continue for 24 hours at room temperature. The product was then dialyzed against an ethanol/water mixture (1:1 v/v) for 24 hours, followed by ultrapure water for 48 hours using dialysis membrane (MWCO-3.5 kDa). The dialyzed product was then lyophilized to obtain hyaluronic acid-oleylamine conjugate (Yield: 57.32%).

To synthesize Chitosan-oleic acid conjugate [237], 210 mg of EDAC HCl, 262 mg of Sulfo-NHS was dissolved in 5 mL of freshly prepared 0.1 M MES buffered saline pH 5.5. Separately, 320 µl of oleic acid (equivalent to 282 mg), was mixed in 1 mL of ethanol and added dropwise in the buffer containing EDAC/Sulfo-NHS mixture. The reaction mixture was kept on stirring for 30 minutes. Then 1080 mg of chitosan oligosaccharide dissolved in 10 mL of 0.1 M MES buffered saline pH 4.7 was added dropwise. The reaction was allowed to continue for 24 hours at room temperature. The reaction mixture was then

dialyzed against ethanol/water (1:1 v/v) mixture for 24 hours followed by ultrapure water for 48 hours using Spectra Por®7 dialysis membrane (MWCO-1000 Da). The dialyzed solution was then lyophilized to obtain Chitosan-oleic acid conjugate (Yield: 61.8%).

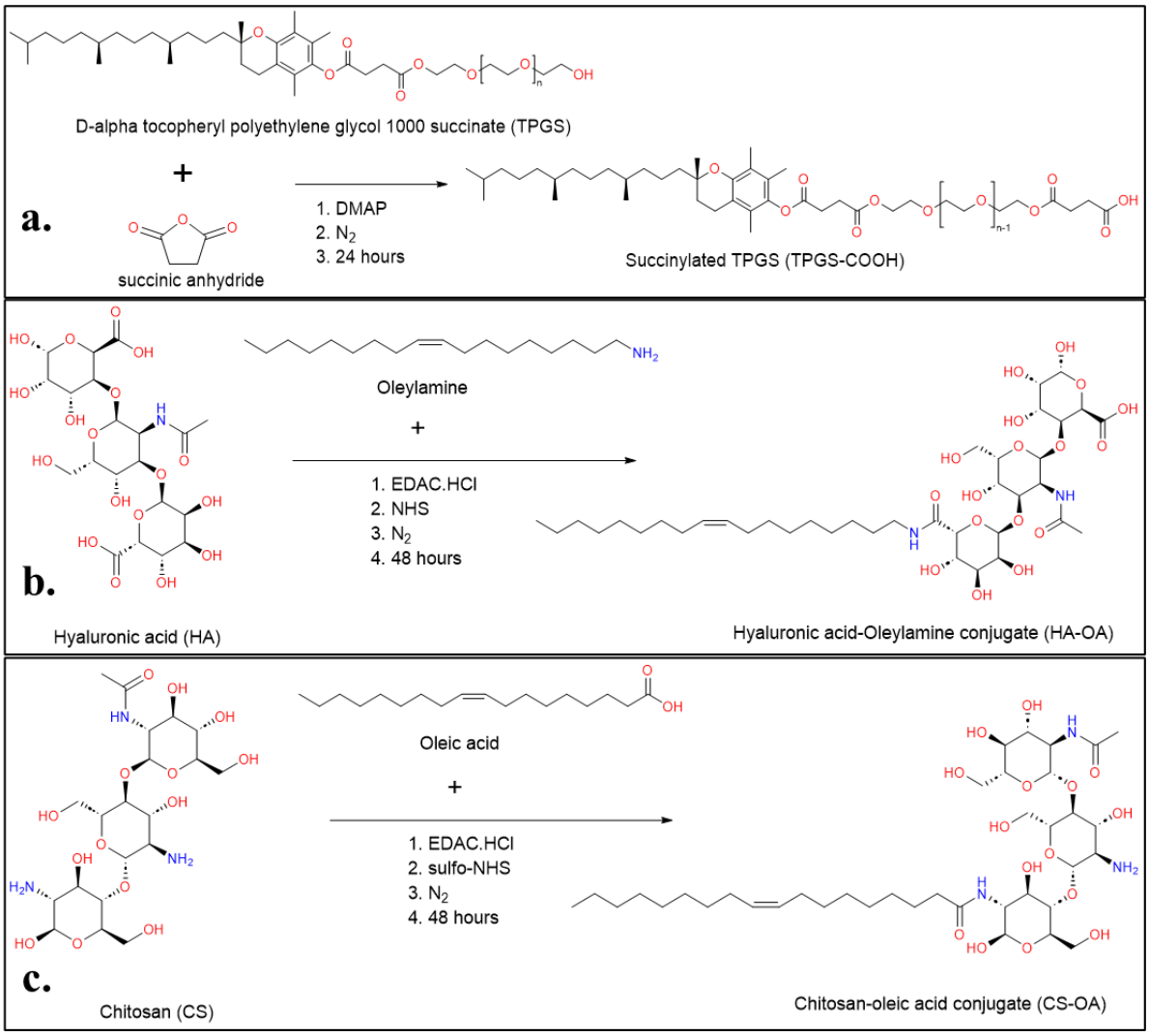

Figure 6.1 Schematic representation of the a) Succinylation of TPGS, b) synthesis of hyaluronic acid–oleylamine conjugate (HA-OA), and c) synthesis of chitosan–oleic acid conjugate (CS-OA).

Carboxylation of terminal hydroxyl group of TPGS was done using succinic anhydride in an inert nitrogen environment [114]. Briefly, 1.5 gram of lyophilized TPGS was dissolved in 30 mL of anhydrous methylene chloride in an oven dried 100 mL Schlenk flask. The solution was degassed using nitrogen. Subsequently, 120 mg of Succinic anhydride and

catalytic amount of DMAP was added to the solution. The flask was sealed with rubber septum and nitrogen filled balloon was used to displace the air inside the flask. The reaction was continued for 48 hours at room temperature. Then the reaction mixture was precipitated in cold diethyl ether to obtain white mass of TPGS-COOH. The precipitate was collected and dialyzed against water/ethanol mixture (1:1 v/v) for 24 hours followed by distilled water for 48 hours using Spectra Por®7 dialysis membrane (MWCO-1000 Da). The dialyzed solution was then lyophilized to obtain white solid mass of TPGS-COOH. (Yield: 64.49%).

6.2.3 Characterization of CS-OA, HA-OA, and TPGS-COOH

Hyaluronic acid (HA), Chitosan oligosaccharide (CS), D-α-tocopheryl polyethylene glycol 1000 succinate (TPGS), Hyaluronic acid-oleylamine conjugate (HA-OA), Chitosan-oleic acid conjugate (CS-OA), and succinylated TPGS (TPGS-COOH) were characterized by 1H-NMR, FTIR, DSC, and XRD analysis. 1H-NMR spectra were recorded using BRUKER AVH D 500 AVANCE III HD 500 MHz NMR Spectrometer at 1024 scans. FTIR spectroscopy was performed using THERMO Nicolet iS5 using KBr pellet method at 64 scans. DSC study was done in Shimadzu DSC-60 Plus at 10 °C min^{-1}. Powder XRD spectra was obtained using Rigaku Miniflex 600 Desktop X-Ray Diffraction System.

6.2.4 Synthesis of HA-OA/CS-OA based nanoparticles

Hyaluronic acid-oleylamine and chitosan-oleic acid conjugate-based nanoparticles were prepared using a modified ionic gelation method [194,238,239]. The use of hyaluronic acid and chitosan based amphiphilic conjugates allows formation of a compact micellar system, thus improving the encapsulation and stabilization of hydrophobic drug in their core. Subsequently, the opposite charge of both the conjugates (CS-OA cationic and HA-OA anionic) leads to formation of nanoparticles by electrostatic interaction [132,240].

Composition of the formulation is detailed in **Table 6.1.** Schematic illustration of the preparation of HA-OA/CS-OA NPT is presented in **Figure 6.2**.

Table 6.1 Composition and properties of various HA-OA/CS-OA NPs prepared during optimization

Formulation	HA-OA (mg)	CS-OA (mg)	TPGS-COOH (mg)	CBT (mg)	CTX (mg)
HA-OA/CS-OA NP1	20	0	10	0	0
HA-OA/CS-OA NP2	20	5	10	0	0
HA-OA/CS-OA NP3	20	10	10	0	0
HA-OA/CS-OA NP4	20	15	10	0	0
HA-OA/CS-OA NP5	20	10	10	2	0
HA-OA/CS-OA NP6	20	10	10	3	0
HA-OA/CS-OA NP7	20	10	10	4	0
HA-OA/CS-OA NP6	20	10	10	5	0
HA-OA/CS-OA NP8	20	10	10	6	0
HA-OA/CS-OA NPT	20	10	10	5	2.5

Firstly, HA-OA and TPGS-COOH was dissolved in 5 mL of ultrapure water. The micellar solution was kept on stirring at 100 RPM and CBT dissolved in 1 mL of methylene chloride was added and probe sonicated using 6mm probe at 60% amplitude for 5 minutes. Methylene chloride was evaporated at room temperature with stirring. Subsequently, CS-OA dissolved in 5 mL of ultrapure water was added dropwise into the solution under constant stirring. The solution was stirred for another 6 hours to obtain HA-OA/CS-OA-based nanoparticles. The nanoparticles were washed thrice and concentrated using Amicon centrifuge filters (MWCO 30 kDa) to obtain HA-OA/CS-OA NP suspension (2 mL). The purified nanoparticles were then lyophilized for various characterization studies. For the preparation of cetuximab-conjugated nanoparticles, before washing, 9.5 mg of EDAC HCl

and 6 mg of NHS was added to the suspension and stirred for 30 minutes. Then, Cetuximab 2.5 mg was added to the suspension and stirred for 3 hours. The cetuximab-conjugated nanoparticles were washed thrice with ultrapure water to obtain HA-OA/CS-OA NPT.

6.2.5 Fabrication of Microneedle

Microneedle array patch was fabricated using micro-molding technique [233,235]. The Schematic illustration of the fabrication of free Cabazitaxel-loaded microneedles (CBT-MN) and HA-OA/CS-OA NPT-loaded microneedles (HA-OA/CS-OA NPT-MN) is presented in **Figure 6.2**. Briefly, a PDMS mold with a square patch of 8 mm × 8 mm size, and 10 × 10 array size, single needle mold height of 600 µm, base width of 200 µm, and a pitch of 500 µm was used to prepare the dissolving microneedles. Polymer blends of various concentrations detailed in **Table 6.2** were prepared.

Table 6.2 Composition of the various formulations used to prepare MNs

Batch	HA (hMW) (mg/ml)	PVA mg/ml	PVP mg/ml	CBT (mg/ml)	HA-OA/CS-OS NPT (eq. CBT) (mg)	Needle Height (µm)
CBT-MN1	100	50	50	2.5	0	567±5.68
CBT-MN2	**80**	**60**	**60**	**2.5**	**0**	**561±5.34**
CBT-MN3	60	70	70	2.5	0	538±5.45
HA-CS-NPT-MN1	**80**	**60**	**60**	**0**	**15 (2.5)**	**546**±3.92
HA-CS-NPT-MN2	80	60	60	0	30 (5)	520±4.73
HA-CS-NPT-MN3	80	60	60	0	60 (10)	498±5.30

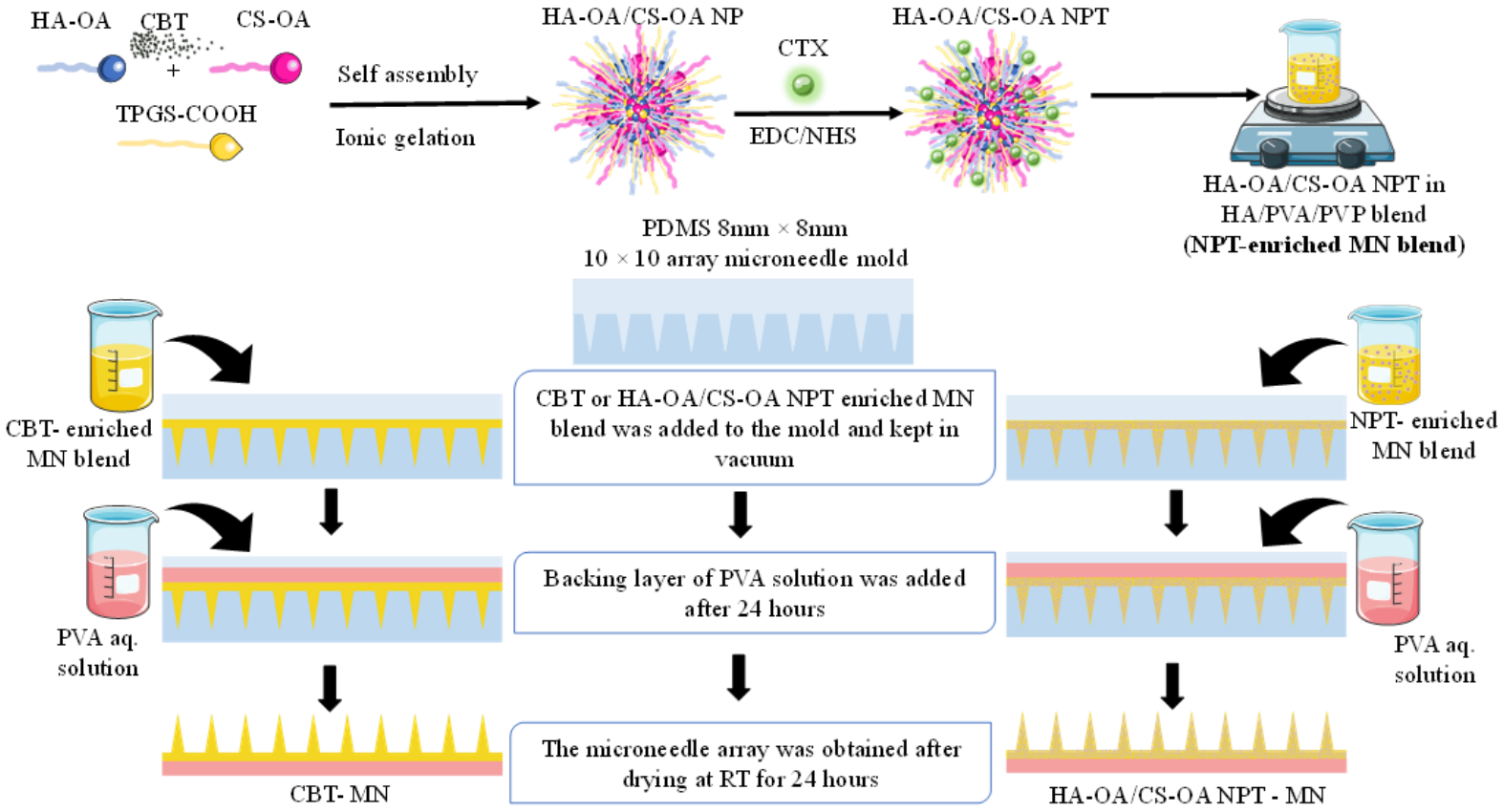

Figure 6.2 Schematic representation of the preparation of non-targeted HA-OA/CS-OA based nanoparticles (HA-OA/CS-OA NPT), targeted HA-OA/CS-OA based nanoparticles (HA-OA/CS-OA NPT), free Cabazitaxel drug loaded microneedles (CBT-MN) and targeted HA-OA/CS-OA based nanoparticles loaded microneedles (HA-OA/CS-OA NPT – MN).

Hyaluronic acid (high MW-HA) and Polyvinyl Alcohol (PVA) were added to ultrapure water and stirred overnight. Then PVP was added to the solution and stirred for another 4 hours. Subsequently HA-OA/CS-OA NPT or CBT was added to the blend and stirred for 2 hours. The prepared blend was then centrifuged at 8000 RPM for 10 minutes to remove the air trapped in the blend. Then 100 µl of the polymer blend was poured in the microneedle mold and kept in vacuum to allow the needle arrays to be filled with the polymer blend. The vacuum was applied for 5 minutes followed by the release of pressure and rest at atmospheric pressure for 1 minute [221]. The process was repeated 4 times to ensure the complete filling of needle arrays with polymer blends without any trapped air. The base polymer blend of 20% PVA was added to form the base. The mold was allowed to dry at atmospheric pressure and room temperature for 24 hours. The formed needle was removed using 3M® microadhesive tape. The microneedle array was stored in a desiccator until further use.

6.2.6 Characterization of HA-OA/CS-OA based nanoparticles

Particle size and zeta-potential of the formulation was assessed using Malvern ZetaSizer. Purified nanoparticles were diluted 10 times using phosphate buffer saline pH 7.4 and scanned to yield the hydrodynamic size and surface charge of the prepared nanoparticles. To determine the encapsulation efficiency, 2 mL of Methanol was added to the purified nanoparticle suspension (2 mL) and probe sonicated in ice bath using 6mm probe at 80% amplitude to disrupt the nanoparticles. The suspension was kept on ultrasonicating bath for 60 minutes and subsequently centrifuged at 12000 RPM for 15 minutes. The supernatant was analyzed using HPLC to determine the concentration and amount of CBT in the suspension. The encapsulation efficiency was determined using the formula mentioned below;

$$Encapsulation\ Efficiency = \frac{Amount\ of\ drug\ detected\ (mg)}{Amount\ of\ drug\ added\ (mg)} \times 100$$

The determine percentage drug loading lyophilized powder of nanoparticles (50 mg) was suspended in 1:1 v/v water: methanol mixture and probe sonicated using 6 mm probe 80% amplitude for 5 minutes in ice bath. Subsequently, the suspension was kept in ultrasonicating bath for 60 minutes at 40 °C. The mixture was centrifuged at 12000 RPM for 15 minutes and supernatant was analyzed using HPLC to determine the concentration of CBT in the supernatant and eventually the amount of drug in 50 mg of nanoparticle. The percentage drug loading was determined using the formula below;

$$Percentage\ Drug\ Loading = \frac{Amount\ of\ drug\ detected\ (mg)}{Amount\ of\ nanoparticle\ (mg)} \times 100$$

Morphology of the nanoparticles was observed using transmission electron microscope (HR- TEM, Tecnai G2 20 TWIN, FEI Corporation of USA (S.E.A.) PTE, LTD) and scanning probe microscope (SPM, NTEGRA Prima, NT-MDT Service and Logistics Ltd). The nanoparticle suspension was diluted 20 times and casted on carbon coated copper grids and dried overnight in vacuum for TEM analysis. For AFM analysis the nanoparticles suspension was drop-casted on the glass grid and dried before analysis.

For solid state characterization, the lyophilized nanoparticles were used. Fourier Transform Infrared Spectroscopy (FTIR) was performed by KBr pellet method using SHIMADZU 8400S, Tokyo, Japan. Microneedles were cut using a scalpel and mixed with KBr. The spectra of CBT, polymers, HA-OA/CS-OA NP, HA-OA/CS-OA NPT, CBT-MN, HA-OA/CS-OA NPT-MN were recorded in the range of 4000-400 cm^{-1}. Similarly, Rigaku Miniflex 600 powder x-ray diffractometer was used to record the X-ray diffraction pattern of all the formulations and drug at 5° min^{-1} with step width of 0.02° in the range of 5-50° of 2θ. The differential scanning calorimetry was done using Shimadzu DSC-60 Plus in the range of 0-250 °C at 10 °C min^{-1}. X-ray photon spectroscopy was conducted using K-

Alpha model (Thermo Fisher Scientific) to assess the surface elemental distribution and changes in surface characteristics of the prepared nanoparticles. The conjugation of Cetuximab was confirmed by Bradford assay.

6.2.7 In vitro drug release of HA-OA/CS-OA based nanoparticles

Dialysis membrane method was used to evaluate the drug release behavior of the fabricated nanoparticles. Freshly prepared washed and purified nanoparticles (eq. to 5 mg of CBT) were concentrated to 2 mL and loaded in a dialysis bag (MWCO 1 kDa) and immersed in 20 mL of PBS pH 7.4. The system was maintained at 100 RPM and 37±0.5 °C throughout the study. Sample of 200 µl was collected at pre-determined time intervals and replaced by fresh buffer. The samples were centrifuged at 12000 RPM and 20 µl of supernatant was injected in HPLC to estimate the amount of drug release at the time point the sample was withdrawn. The study was also conducted in acetate buffer pH 5.8.

6.2.8 Cell culture studies

6.2.8.1 Cell line maintenance:

The MDA-MB-231 cell line was grown in a humidified CO2 incubator at 37 °C using DMEM supplemented with FBS (fetal bovine serum) and penicillin-streptomycin antibiotic solution.

6.2.8.2 In vitro cytotoxicity assay:

1×10^6 MDA-MB-231 cells were seeded in a 96-well cell culture plate. After adherence and gaining proper morphology, cells were treated with different concentrations of neat CBT, HA-OA/CS-OA NP, and HA-OA/CS-OA NPT. After treatment, the cells were incubated for 24 hours. Afterward, the used media were discarded and 100 µl MTT containing media was added in each well. After 2 hours of incubation MTT containing media was discarded and 100 µl of DMSO were added in each well to dissolve the purple-

colored formazan crystals. The absorbance of the dissolved formazan in each well was measured using a microplate reader at 570 nm to estimate the viability of cells [241].

6.2.8.3 Cellular uptake:

The cellular uptake study was conducted using coumarin-6 (CM6) doped formulations. 5×10^4 MDA-MB-231 cells were seeded in a 12-well cell culture plate. After incubation the cells were treated with free CM6/CBT solution, HA-OA/CS-OA NP, HA-OA/CS-OA NPT at concentrations equivalent to IC_{50} value of HA-OA/CS-OA NPT (CM6 ~0.1 µg/ml) and left for 6 hours of incubation in a humidified CO_2 incubator. To confirm the role of EGFR in endocytosis of HA-OA/CS-OA NPT, one group received cetuximab pretreatment (30 mins before HA-OA/CS-OA NPT treatment). Further, the nuclei of the cells were counterstained with Hoechst33342 for 10 minutes. Subsequently, cells were washed with PBS and imaged using the EVOS FL Cell Imaging System [124].

6.2.8.4 Hoeschst/PI staining:

5×10^4 cells were seeded in a 12-well culture plate and allowed to adhere. After adherence, cells were exposed to the aforementioned formulations at concentrations equivalent to the IC_{50} value of HA-OA/CS-OA NPT and further incubated for 24 hours. Subsequently, the used media was removed, and Hoeschst33342/PI stain was added and incubated for 15 minutes. The cells were imaged using the EVOS FL Cell Imaging System at 400X magnification and 100 µm scale bar. [125]

6.2.8.5 Assessment of mitochondrial membrane potential:

5×10^4 MDA-MB-231 cells were seeded in a 12-well cell culture plate. After adherence, cells were exposed to the treatments described above at concentrations equivalent to IC50 value of HA-OA/CS-OA NPT and incubated for 24 hours. The cells were then stained with 0.5 µM concentration of JC-1 dye and incubated for 30 minutes [242]. The images

were captured using the EVOS FL Cell Imaging System at 400X magnification and 100µm scale bar.

6.2.8.6 Cell cycle analysis:

Briefly, 1× 10^6 MDA-MB-231 cells were seeded in a 6-well plate. After adherence, the cells were subjected to the treatments mentioned in the above studies and incubated for 24 hours. Subsequently, the cells were harvested using 1mM EDTA, fixed using 80% ethanol, and left for overnight incubation at -20ºC. The cells were then centrifuged at 3000 rpm for 7 minutes and staining buffer (0.1 mg/ml RNase A and 0.05 mg/ml propidium iodide in 0.1 % Triton X-100 containing PBS) was added to the cells after discarding the supernatant. The cells were then further incubated at 37 ºC for 10 minutes and analyzed using flow cytometry. [242]

6.2.9 Evaluation of MN

6.2.9.1 Microscopy

The microneedles were adhered to sample holder using double-sided tape, gold coated using sputter coater and imaged by SEM.

6.2.9.2 Dissolution of Microneedles

Microneedle dissolution was assessed using a 24-well plate. Briefly, using a double-sided adhesive tape the microneedle array was immersed upside down in 2 ml of PBS pH-7.4, at 37°C and 100 rpm stirring. At predetermined time intervals 200µl of media was withdrawn and replaced by fresh media. To the withdrawn sample, 100µl of methanol was added and the solvent was evaporated using rotary evaporator. The dried sample was resuspended in 200 µl of methanol and sonicated for 15 minutes followed by centrifugation at 6000 RPM for 5 mins. 20 µl of supernatant was then injected in HPLC to determine the amount of drug/drug loaded nanoparticle release from the microneedle.

6.2.9.3 Quantification of drug content in needle array

The microneedle array was dipped from the needle side in 2 mL of water-methanol mixture (1:1 v/v) according to the dissolution time (5 mins). The solution then sonicated to dissolve the drug encapsulated in nanoparticles for 30 minutes and filtered using a syringe filter (0.2 µm pore size). The filtered solution was then analyzed using HPLC to determine the amount of drug loaded in one microneedle array.

6.2.9.4 In vitro and ex vivo skin insertion study

In vitro permeation study was done using multiple layers of Parafilm (thickness 127 µm). Briefly, 6 layers of parafilm were stacked and kept on a stryrofoam base. The microneedle array was pressed onto the stacked parafilm using thumb for 1 minute. Various layers of parafilm were studied using optical microscope and number of holes created in every layer was observed. The graph was plotted for percentage holes created against the layer of parafilm and apparent depth of permeation. Skin penetration of needles was also calculated by inserting the microneedle array into the excised rat skin and held in than position for 1 minute. The skin penetration was checked by histological study.

For *ex vivo* assessment drug permeation, a 7.5ml jacketed Franz diffusion assembly was used with a 450 µm thickness rat skin sample sandwiched between receptor and donor chamber. The receptor chamber was filled with 7.5 mL of PBS pH 7.4, maintained at 37 °C and 50 rpm. The system was allowed to equilibrate and microneedles (CBT-MN and HA-OA/CS-OA NPT-MN) were inserted manually into the skin. The aliquots were collected from the receptor compartment at pre-determined time intervals and analyzed using HPLC. For comparison, drug and nanoparticle loaded polymer blend were also applied on the skin and assessed for drug permeation. After 48 hours, topical surface was washed and drug concentration in skin samples were determined by extracting the drug from tissue homogenate.

6.2.10 In vivo efficacy: tumor regression, survival analysis, and histological studies

A tumor regression study was performed in DMBA-induced tumor-bearing female SD rats [243]. Animals were divided into four groups (n=5). Group 1 was the control group and received no treatment, while Group 2 received an intravenous dosage of CBT (5 mg/kg). However, in groups 3 and 4, microneedles were inserted manually into the skin. Group 2 received three dosages per week (a total of 6 dosages), while in groups 3 and 4, a microneedle array was inserted each day for 14 days. Tumor diameter in 3 different planes was determined using Vernier Caliper at day 0, 4, 7, 10, and 14, and the mean of three values of diameter/2 was used as "r". The volume was determined using the formula below, where r is the average radius of the tumor.

$$Tumor\ volume = \frac{4}{3}\Pi r^3$$

Tumors were collected for histological analysis and washed with cold phosphate-buffered saline (pH 7.4). The tissue was fixated using 10% buffered formalin. The fixated samples were dehydrated, treated with xylene, and embedded in paraffin. The tissue sections from the embedded samples were obtained, deparaffinized, and stained using Hematoxylin. Subsequently, the tissue is counterstained using Alcoholic Eosin, dehydrated with ethanol, and cleared with xylene. The tissue was then mounted under a coverslip and observed under light microscope.

For survival analysis, Group 5 (n=5) consisting of healthy female SD rats were also included. All the groups receive treatment as mentioned above. The animals were housed for 120 days and dignified survival was calculated on 120th day [244].

6.2.11 Statistical analysis

The results were reported as Mean ± standard deviation (SD). For comparison of results and groups, t test (non-parametric), one-way ANOVA and two-way ANOVA at p values of *p<0.05, **p<0.01, ***p<0.001, and ****p<0.0001 were used. All statistical analysis

were performed using software GraphPad Prism 9.0.0 (GraphPad Software, San Diego, CA, USA).

6.3 Results and discussion

6.3.1 Synthesis and characterization of CS-OA, HA-OA, and TPGS-COOH

For preparation of nanoparticles, amphiphilic conjugates of hyaluronic acid with oleylamine and chitosan with oleic acid were first synthesized using carbodiimide chemistry. The synthesis of HA-OA, and CS-OA, was confirmed by 1H NMR (**Figure 6.3 Figure 6.4**) and FTIR (**Figure 6.5**). The successful succinyl of TPGS was confirmed earlier in the **section 4.3.1** (**Figure 4.65** to **Figure 4.8**).

In FTIR spectrum, characteristic peaks for TPGS **(Figure 6.5)** were observed at 3503 cm^{-1} (terminal -OH group), 2910 cm^{-1} (alkyl -CH stretching bond of aliphatic parts of the molecule), 1744 cm^{-1} and 1643 cm^{-1} (-C=O stretching vibration), 1458 cm^{-1} (–C=C– peak of aromatic ring), 1352 cm^{-1} (peculiar peak of $–CH_2$ group of PEG chain), 1251 and 1113 cm^{-1} (-C-O- stretching peaks). For TPGS-COOH, peaks were also observed at 3501 cm^{-1} (terminal hydroxyl functional band), 2908 cm^{-1} (–CH stretching vibration of the methyl group), 1734 cm^{-1} (strong –C=O stretching vibration with increased transmittance) and peak at 1641 cm^{-1} confirmed successful synthesis of TPGS-COOH. Other peaks were also observed at 1455 cm^{-1} (–C=C– peak of aromatic ring), 1353 cm^{-1} ($–CH_2$ peak of PEG chain), and 1110 cm^{-1} (-C-O- stretching).

The 1H-NMR spectra of Hyaluronic acid showed characteristic proton of acetamide at 1.8 ppm, multiple peaks in the range of 4.0-3.0 ppm, and anomeric proton at 4.57 ppm (**Figure 6.3**). The peaks of oleylamine were observed at 5.32 (a), 2.48 (b), 1.95 (c), 1.28 (d), and 0.88 (e) ppm. The HA-OA conjugate showed characteristic proton of acetamide at 1.8 ppm, multiple peaks in the range of 4.0-3.0 ppm, and anomeric proton at 4.57 ppm. The peaks of oleylamine were observed at 5.32 (a), 2.48 (b), 1.95 (c), 1.28 (d), and 0.88

(e) ppm. The HA-OA conjugate exhibited the characteristic acetamide peak of HA at 2.08 ppm, HA backbone in the range of 4.8-2.8 ppm, and oleylamine peaks at 5.33, 2.89, 2.30, and 1.4-0.8 ppm.

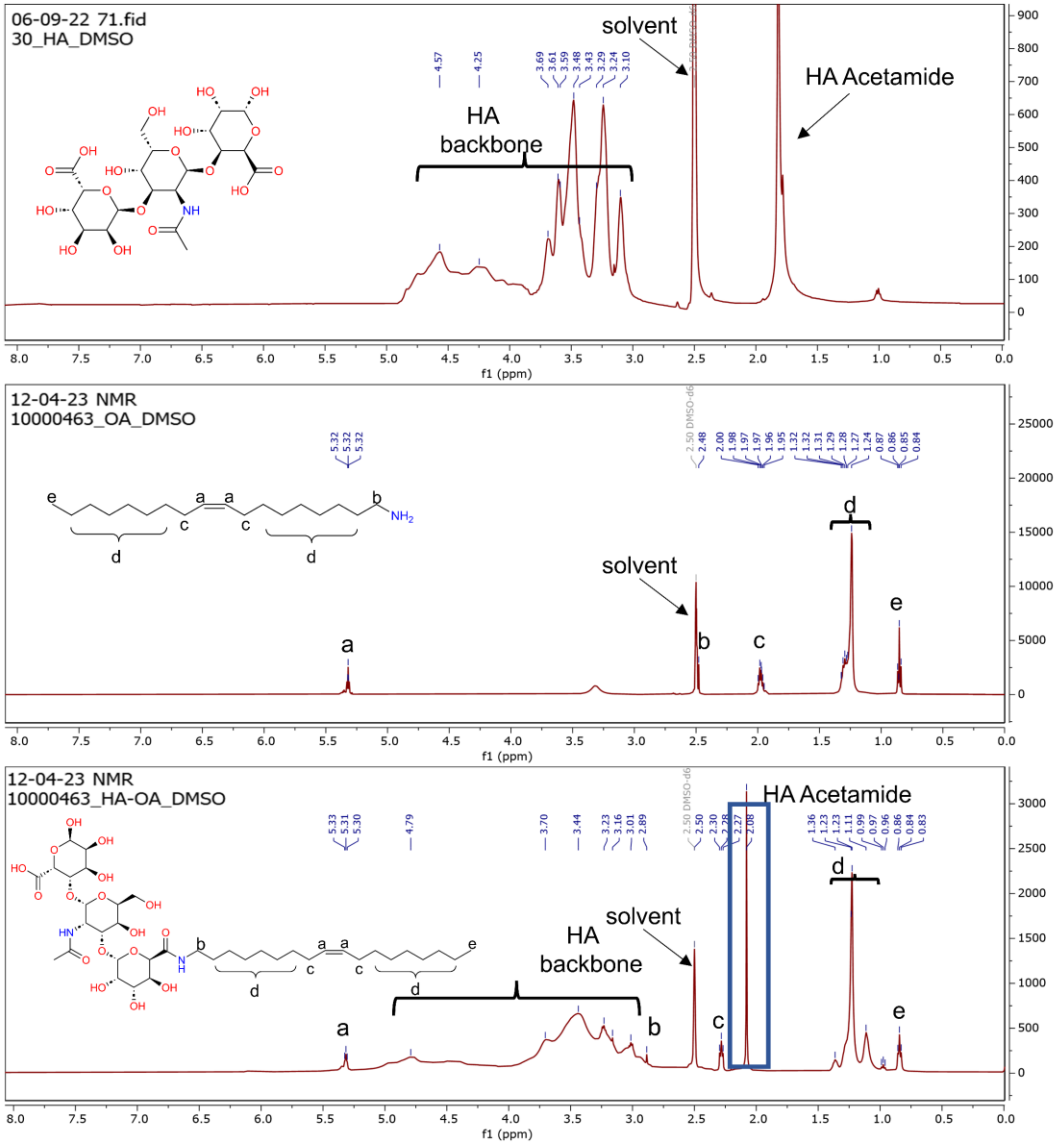

Figure 6.3 ^{1}H NMR spectra of Hyaluronic acid, oleylamine (OA), and HA-OA.

The aliphatic oleylamine peaks exhibited a minor downfield shift after conjugation with HA backbone. FTIR spectrum of HA **(Figure 6.5)** showed characteristic band at 3450 cm^{-1} (-OH stretching), 2919 cm^{-1} (symmetric methyl -C-H stretch), 1743 cm^{-1} (-C=O of -COOH), 1635 cm^{-1} (acetamide), 1413 cm^{-1} (C-O stretching of COO-), 1377 cm^{-1}, 1317 cm^{-1}, 1155 cm^{-1}, and 1037 cm^{-1} (C-O-C hemiacetalic system of saccharide units)

[245,246]. HA-OA showed FTIR band at 3408 cm^{-1} (-OH stretching of HA), 2925 cm^{-1} (OA) 2853 cm^{-1} (OA), 1740 cm^{-1}(OA), 1639 cm^{-1} (acetamide of HA), 1553 cm^{-1}, 1438 cm^{-1} (OA), 1374 cm^{-1}, 1303 cm^{-1}, 1156 cm^{-1} and 1058 cm^{-1}.

As shown in **Figure 6.4,** ^{1}H NMR of chitosan had characteristic anomeric proton peak at 4.84 ppm (C1). The multiple peaks between 4.03-2.6 ppm were of protons of glucosamine subunits (CSO Backbone) while protons of acetyl groups attached to the glucosamine (C2) was observed at 1.8 ppm.

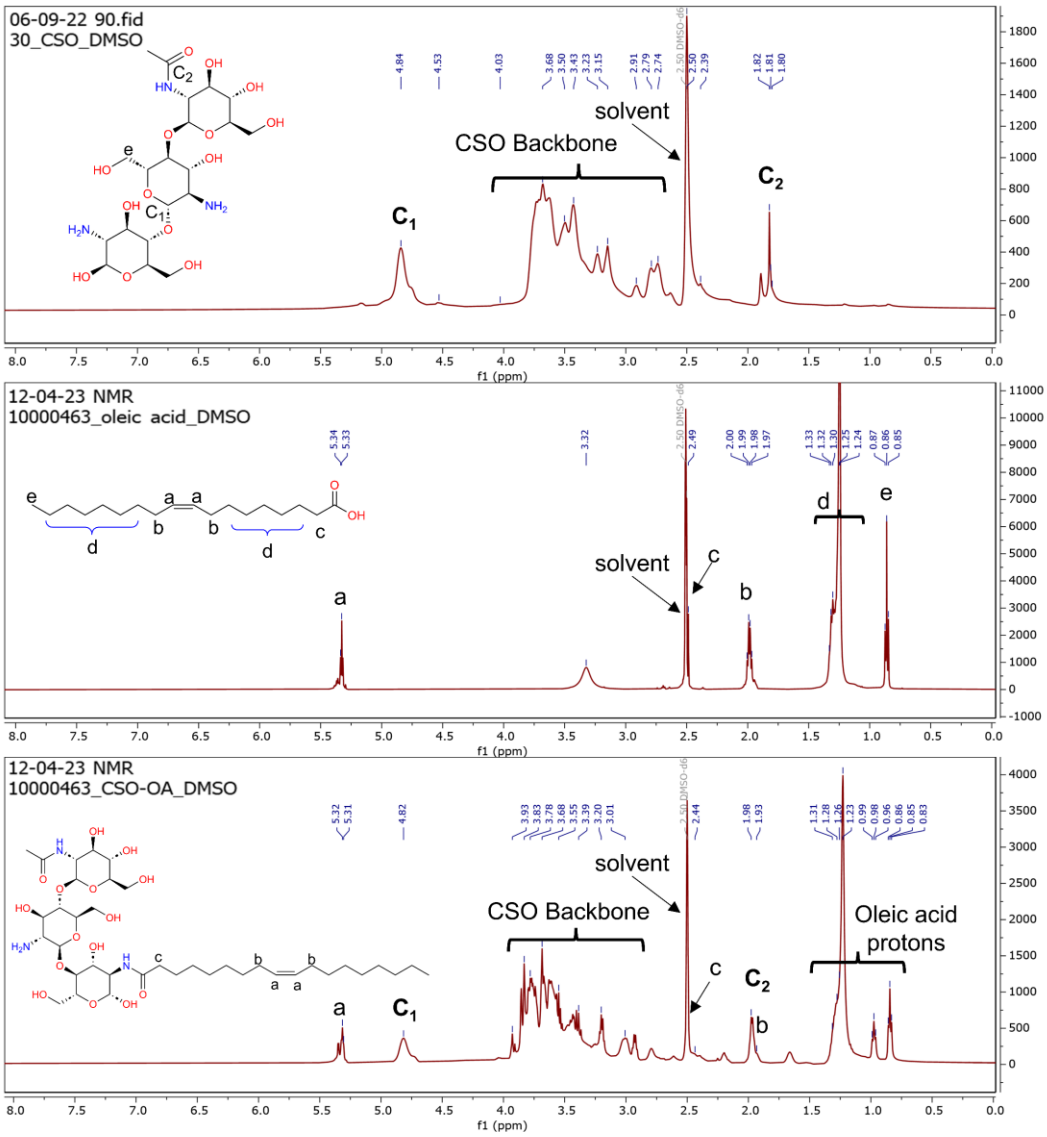

Figure 6.4 ^{1}H NMR spectra of Chitosan (CSO), Oleic acid (OA), and CS-OA.

The characteristic peaks of oleic acid were at 5.34 (a), 2.49 (c), 1.99 (b), 1.4-1.2 (d), and 0.86 (e) ppm. After conjugation, the CS-OA exhibited the characteristic anomeric peak of chitosan (C1) at 4.82 ppm, protons of unsaturated carbon of oleic acid at 5.32 (a) ppm, proton of acetyl group of glucosamine at 1.98 (C2) ppm, and oleic acid protons in the range of 1.3-0.8 ppm. Also, the sharpened proton signals of the chitosan backbone in the range of 4.0-3.0 ppm may be attributed to the improved solubility of chitosan in DMSO after conjugation.

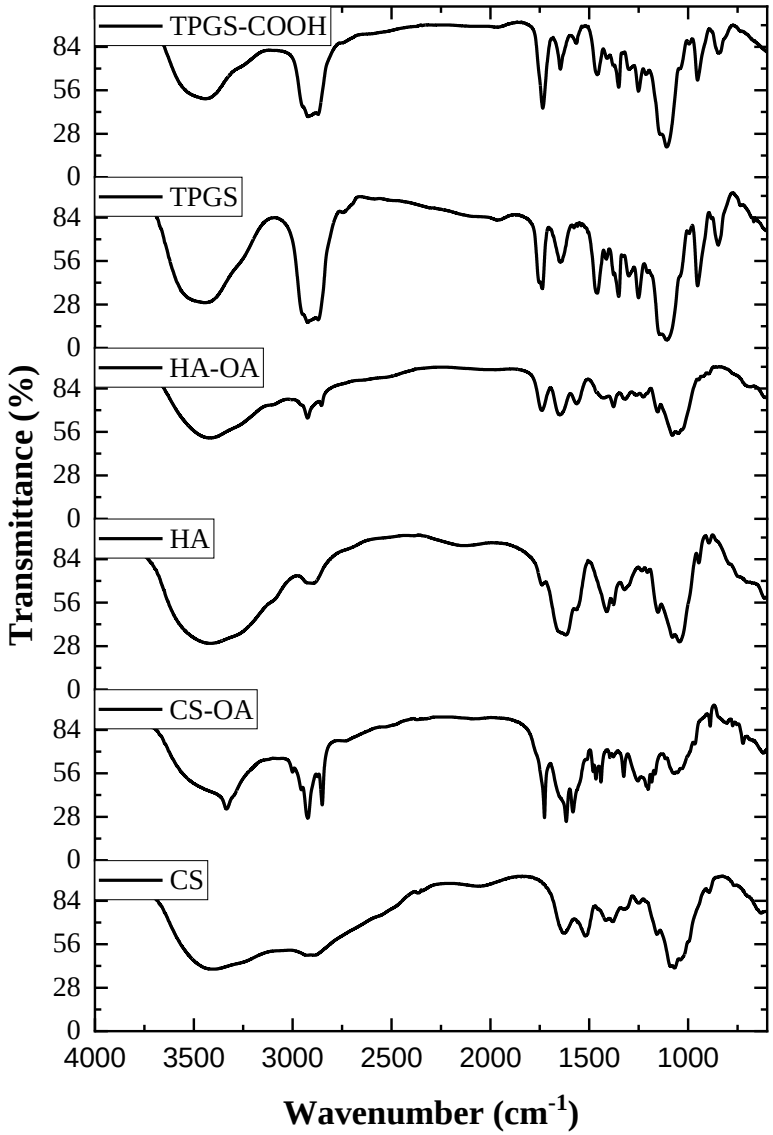

Figure 6.5 FTIR spectrum of CS, CS-OA, HA, HA-OA, TPGS, and TPGS-COOH

FTIR spectra **(Figure 6.5)** of chitosan (CS) exhibited characteristic peak at 3452 cm^{-1} as broad peak for hydroxyl (-OH) stretching and NH_2 group, 2925 cm^{-1} for C-H stretching, 1634 cm^{-1} for C=O stretching vibrations of N-acetylated unit of chitosan, 1520 for -NH bending, 1151 and 1073 cm^{-1} for C-O-C stretching vibrations. CS-OA also had peaks at 3335 cm^{-1} (hydroxyl (-OH) stretching and NH_2 group of CS), 1616 cm^{-1} (C=O stretching vibrations of N-acetylated unit of CS), 1579 cm^{-1} (-NH bending of CS), 1440 cm^{-1}, 1325 cm^{-1}**,** 1259 cm^{-1}, 1203 cm^{-1}, 1055 cm^{-1} (C-O-C stretching vibrations of CS) and 888 cm^{-1}. While peak at 1726 cm^{-1} of -C=O stretching confirmed introduction of acyl group. Peaks at 2925 cm^{-1}, 2849 cm^{-1}, and 1466 cm^{-1} was also attributed to aliphatic chain of oleic acid.

6.3.2 Formulation and characterization of nanoparticles

Synthesized conjugates of HA-OA, CS-OA, TPGS-COOH were used to synthesize a hybrid self-assembled nanoparticles loaded with CBT. The common hydrophobic aliphatic chain in the form of oleic acid in CS-OA and oleylamine in HA-OA creates a stable micellar structure that interacts due to the opposite charge on both the conjugates to form a hybrid self-assembled nanoparticle via. ionic gelation. The amphiphilicity of the conjugates can also improve the loading efficiency of hydrophobic CBT. Incorporation of TPGS-COOH further provided stability to the formed nanostructure and aided in post conjugation of targeting ligand on the surface via. amide linkage. Also, TPGS-COOH has inherent P-gp inhibitory activity that equips the nanoparticles to overcome the efflux-mediated resistance [247].

Table 6.3 Particle size, PDI, zeta potential, EE, and DL of prepared nanoparticles.

Formulation	Hydrodynamic Size (nm)	PDI	Zeta potential (mV)	EE (%)	DL (%)
HA-OA20/TPGS10 NP1	290±6.73	0.373±0.08	-40.7±4.3	--	--
HA-OA20/CS-OA5/TPGS10 NP2	168±5.47	0.184±0.02	-24.6±3.1	--	--
HA-OA20/CS-OA10/TPGS10 NP3	104±4.62	0.161±0.01	-10.3±3.0	--	--
HA-OA20/CS-OA15/TPGS10 NP4	268±19.38	0.428±0.07	-5.3±2.92	--	--
HA-OA/CS-OA (NP5)	108±3.19	0.154±0.03	-10.6±2.6	89.5±1.17	6.83±1.92
HA-OA/CS-OA NP6	114±4.06	0.128±0.02	-10.3±4.1	89.37±0.9	9.94±2.36
HA-OA/CS-OA NP7	112±2.94	0.139±0.03	-10.4±2.2	89.46±1.3	12.78±1.9
HA-OA/CS-OA NP8	**111.9±3.40**	**0.147±0.01**	**-10.1±2.8**	**86.56±1.5**	**15.09±2.1**
HA-OA/CS-OA NP9	120.1±4.25	0.157±0.03	-10.3±4.1	80.33±3.2	15.07±1.9
HA-OA/CS-OA NPT	**125.5± 5.16**	**0.212±0.02**	**-9.49±5.4**	**86.19±1.9**	**14.27±2.5**

Data presented as Mean ± SD; n=6

Optimization of HA-OA and CS-OA ratio was performed to optimum particle size, zeta potential, and drug encapsulation (data in **Table 6.3**). The weight ratio of 2:1 HA-OA:CS-OA yielded optimum characteristics like, mono-dispersed particles and high drug loading (**Table 6.3**).

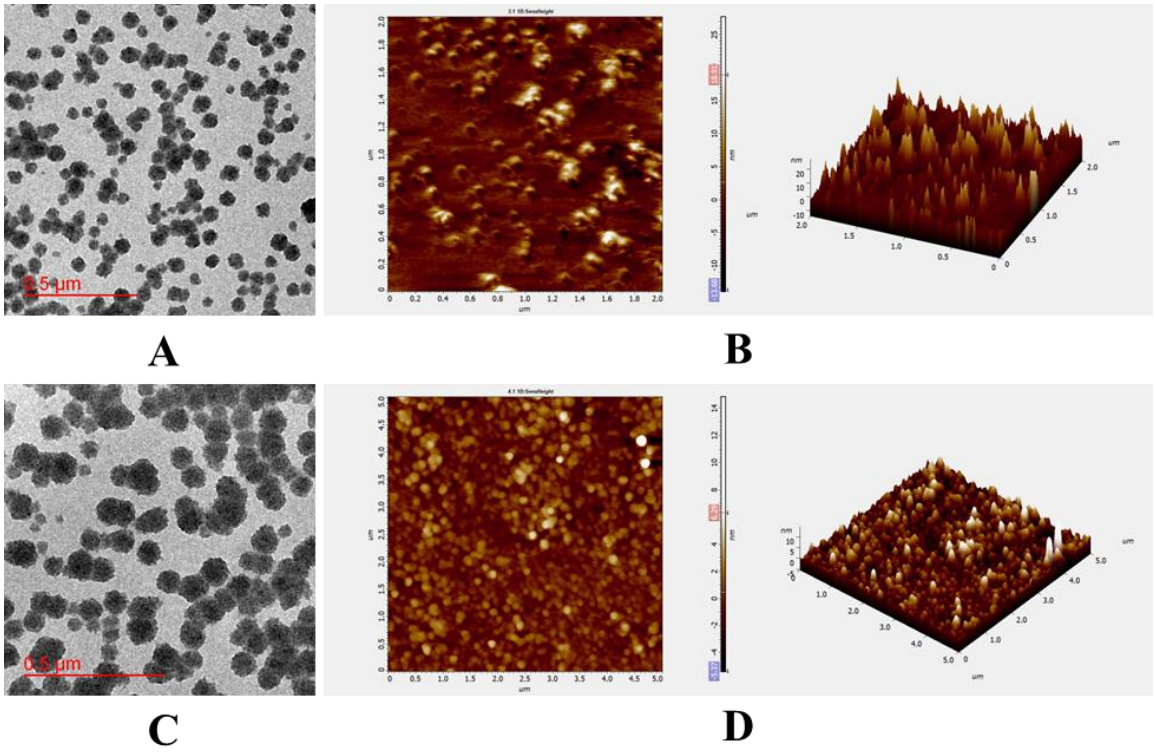

Figure 6.6 Characterization of HA-OA/CS-OA based hybrid nanoparticles; (**A)** TEM image of HA-OA/CS-OA NP (**B**) AFM image of HA-OA/CS-OA NP, (**C**) TEM image of HA-OA/CS-OA NPT, and (**D**) AFM image of HA-OA/CS-OA NPT.

Optimal formulation of HA-OA/CS-OA NP (NP8) exhibited particle size, PDI, and zeta potential of about 111.9±3.40 nm, 0.147±0.013, and -10.1±2.83mV. The hydrodynamic size of HA-OA/CS-OA NPT was higher (125.5± 5.16 nm) due to the conjugation of antibody on nanoparticles surface but the particles remained monodispersed (PDI=0.212±0.020). A trend of decreasing zeta potential was observed with the increase in CS-OA fraction due to the inherent positive charge of the CS-OA conjugate. The microscopic assessment using TEM (**Figure 6.6 A&C**) and AFM (**Figure 6.6 B&D**) also

exhibited spherical morphology of formed nanoparticles (HA-OA/CS-OA NP & HA-OA/CS-OA NPT) that conforms with the hydrodynamic size.

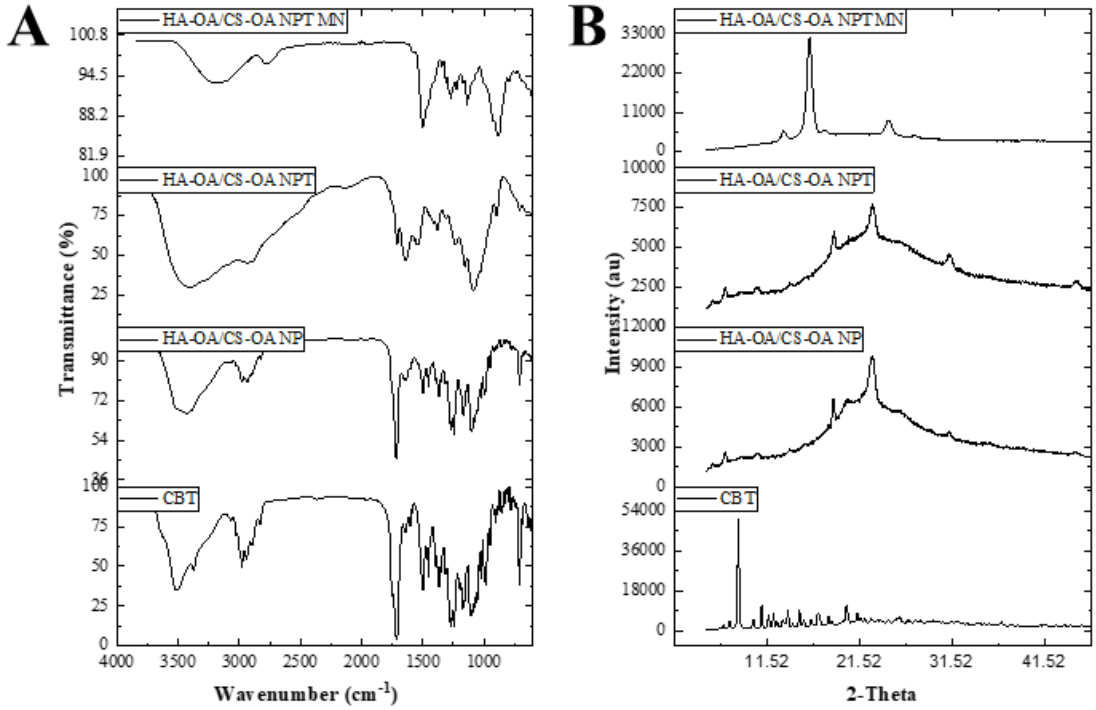

Figure 6.7 (A) FTIR and **(B)** XRD spectra of CBT, HA-OA/CS-OA NP, HA-OA/CS-OA NPT, and HA-OA/CS-OA NPT MN.

The FTIR spectra of CBT, HA-OA/CS-OA NP and HA-OA/CS-OA NPT were as shown in **Figure 6.7A**. The characteristic peaks of CBT were 2982 cm^{-1} (a strong peak for N-H stretching of 2˚ amine) and 711 cm^{-1} (C-H stretching of aromatic C) [105]. HA-OA/CS-OA NP exhibited peaks at 3494 cm^{-1}, 2979 cm^{-1}, 2934 cm^{-1}, 2889 cm^{-1}, 2815 cm^{-1}, 1716 cm^{-1}, 1650 cm^{-1}, 1493 cm^{-1}, 1451 cm^{-1}, 1368 cm^{-1}, 1270 cm^{-1}, 1242 cm^{-1}, 1172 cm^{-1}, 1104 cm^{-1}, 999 cm^{-1}, and 646 cm^{-1}. The peaks for HA-OA/CS-OA NPT were at 3421 cm^{-1}, 2950 cm^{-1}, 2885 cm^{-1}, 1710 cm^{-1}, 1639 cm^{-1}, 1535 cm^{-1}, 1375 cm^{-1}, 1231 cm^{-1}, 1157 cm^{-1}, 1095 cm^{-1}, and 898 cm^{-1}. The peaks observed in both nanoparticles were corresponding to characteristic peaks of HA-OA, CS-OA, and TPGS-COOH. The

characteristic sharp peaks of the drug were masked in nanoparticles, suggesting encapsulation of drug in nanoparticles.

The X-Ray diffraction pattern (**Figure 6.7B**) for CBT showed characteristic peaks at 2θ = 7.274˚, 7.779˚, 8.880˚, 10.163˚, 12.497˚, 12.809 ˚, 13.265˚, 14.324˚, 15.124˚, 15.585˚, 16.470˚, 16.945˚, 17.636˚, 18.680˚, 19.386˚, 21.035˚, 23.052˚, 23.438˚, 26.987˚, 30.099˚, 30.664˚, 32.230˚, and 33.525˚. The XRD spectra of CBT was similar to previous reported value revealing crystalline nature of the drug [210]. The XRD spectrum of HA-OA/CS-OA NP showed two major peaks at 19.311˚ and 23.451˚ corresponding to TPGS-COOH. The diffraction pattern was similar to CS-OA and HA-OA with a broad spectrum revealing amorphous nature of nanoparticles. HA-OA/CS-OA NPT also exhibited peaks at 19.230˚ and 23.470˚ with diffraction pattern similar to HA-OA and CS-OA. The peaks of CBT were mask in both formulations indicating the encapsulation of the drug in nanoparticles.

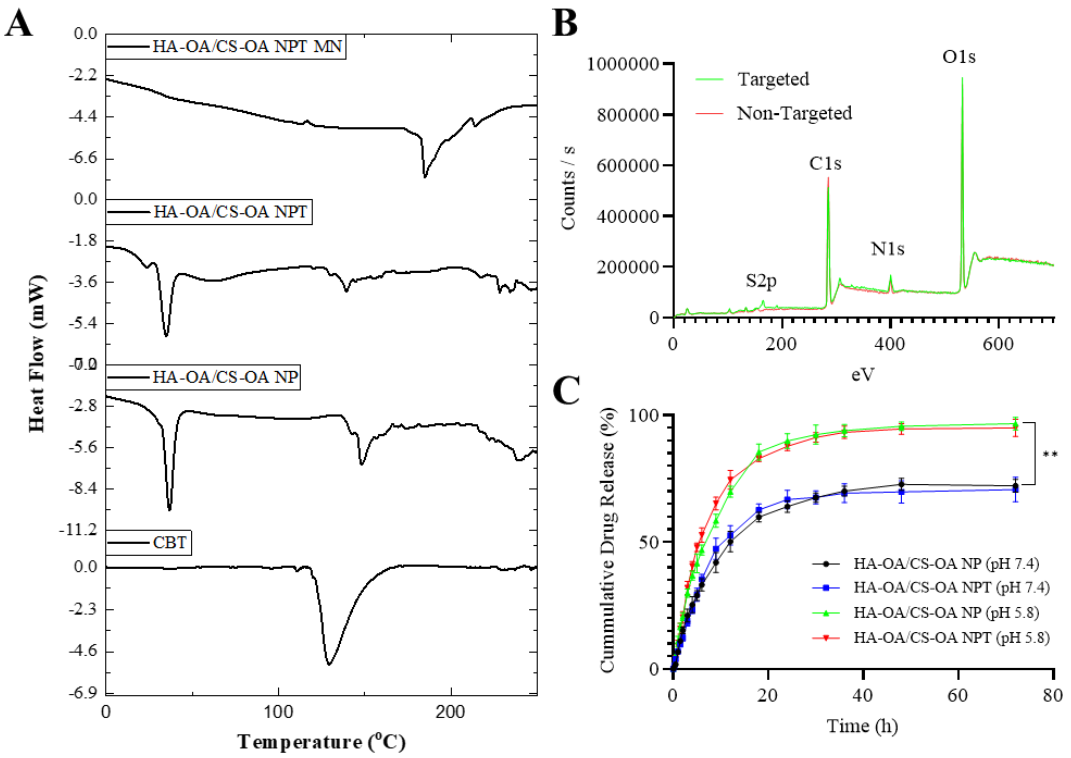

Figure 6.8 (A) DSC thermogram of CBT, HA-OA/CS-OA NP, HA-OA/CS-OA NPT, and HA-OA/CS-OA NPT-MN. **(B)** Surface characterization by XPS analysis of HA-OA/CS-

OA NP and HA-OA/CS-OA NPT. **(C)** *In vitro* drug release study of HA-OA/CS-OA NP and HA-OA/CS-OA NPT at pH 5.8 and pH 7.4.

Figure 6.8(A) showed the DSC thermogram of CBT, HA-OA/CS-OA NP, and HA-OA/CS-OA NPT. CBT exhibited an endothermic peak at 130.50 ℃ owing to its crystalline nature [248]. HA-OA/CS-OA NP showed two endothermic peaks at 36.59℃ and 148.30 ℃. HA-OA/CS-OA NPT also had two endothermic peaks at 35.15 ℃ and 139.524 ℃. The first endothermic peak observed in thermogram of both nanoparticles was of TPGS-COOH while second endothermic peak was attributed to release of water molecules from nanoparticles formed by ionic gelation [249]. The ionic gelation of HA-OA and CS-OA caused hindrance in the release of water from the nanoparticles, causing the peak to shift rightward. In addition, the masking of the endothermic of CBT may be attributed to its encapsulation in nanoparticles.

The XPS analysis was conducted for elemental and surface analysis of prepared nanoparticles (**Figure 6.8(B)**). Results revealed higher proportion of O1s and N1s in HA-OA/CS-OA NPT (O1s; 32.15 and N1s; 5.53%) than HA-OA/CS-OA NP (O1s; 29.32 and N1s; 4.09%). Also, a minor S2p signal in HA-OA/CS-OA NPT (S2p; 0.92%) was observed that was negligible in HA-OA/CS-OA NP (S2p; 0.02%). A marked increase in N1s and presence of S2p signals indicated the conjugation of cetuximab on the nanoparticle surface. The monoclonal antibody is comprised of amino acid sequences with high nitrogen and sulfur presence. This indicated successful conjugation of Cmab on the surface of HA-OA/CS-OA NP. The conjugation of Cmab on the surface of nanoparticles was also confirmed by Bradford assay. The degree of conjugation was found to be 72.74%± 4.81.

Table 6.4 Fitted release kinetic model for in-vitro drug release of nanoparticles.

Model	HA-OA/CS-OA NP 7.4	HA-OA/CS-OA NPT 7.4	HA-OA/CS-OA NP 5.8	HA-OA/CS-OA NPT 5.8
Zero Order	0.3872	0.3310	0.2985	0.2078
First order	0.8779	0.8547	0.9961	0.9902
Higuchi	0.9053	0.8724	0.8810	0.8456
Korsmeyer-Peppas	0.9303	0.9038	0.9216	0.9050
Hixson-Crowell	0.8094	0.7807	0.9309	0.8898
Hopfenberg	0.8778	0.8545	0.9961	0.9902
Baker-Lonsdale	0.9526	0.9286	0.9539	0.9396
Makoid-Banakar	0.9941 n = 0.704 AIC = 83.36 MSC = 4.68	0.9870 n = 0.738 AIC = 97.93 MSC = 3.89	0.9929	0.9833
Weibull	0.9860	0.9700	**0.9982** **β = 0.877** **AIC = 72.10** **MSC = 5.88**	**0.9971** **β = 0.715** **AIC = 81.08** **MSC = 5.37**
Logistic	**0.9981** **β = 2.719** **AIC = 63.08** **MSC = 5.81**	**0.9977** **β = 3.343** **AIC = 66.78** **MSC = 5.62**	**0.9967** **β = 2.768** **AIC = 83.43** **MSC = 5.25**	**0.9997** **β = 3.083** **AIC = 42.59** **MSC = 7.51**
Gompertz	**0.9948** **β = 1.313** **AIC = 78.99** **MSC = 4.93**	**0.9867** **β = 1.350** **AIC = 96.24** **MSC = 3.99**	0.9810	0.9945

AIC = Akaike Information criteria, best fit with lowest value. MSC = Model selection criteria, Larger MSC means better fit.

6.3.3 In vitro drug release study

In vitro drug release study conducted for prepared nanoparticles in pH 7.4 showed drug release at a lower rate compared to pH 5.8 (**Figure 6.8(C)**). The HA-OA/CS-OA NP released only 33.12±2.38 % drug in 6hr and 72.19±2.54% in 72h. HA-OA/CS-OA NPT showed drug release of 35.31±1.89 % drug in 6h and 70.68±4.87% in 72h. However, at acidic pH the drug release rate increased to 46.86±2.05% and 52.79±2.83 % in 6h by HA-OA/CS-OA NP and HA-OA/CS-OA NPT, respectively. Also, at 72h 96.22±2.51% and 95.05±3.33% of the loaded drug was released from HA-OA/CS-OA NP and HA-OA/CS-OA NPT, respectively, which was significantly (**p<0.01) higher than the cumulative release at pH 7.4. The Logistic model and Gompertz model were best fit for the drug release behavior of nanoparticles at pH 7.4 indicating swelling and diffusion-controlled drug release (**Table 6.4**). While nanoparticles at pH 5.8 showed logistic model (swelling controlled diffusion) and Weibull model (erosion controlled diffusion) as best fit [212,213,250].

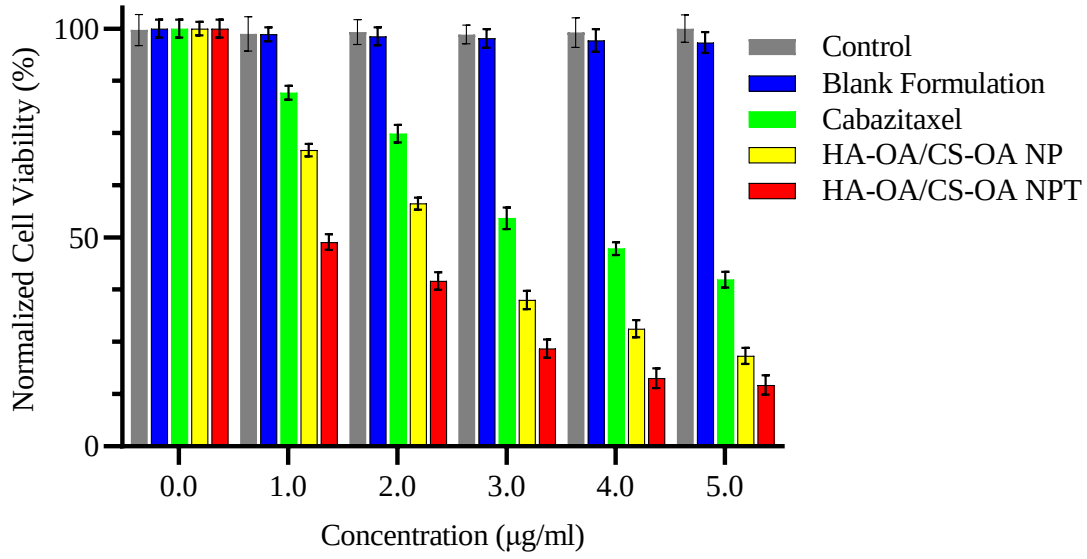

Figure 6.9 *In vitro* cytotoxicity of HA-OA/CS-OA NP and HA-OA/CS-OA NPT in MDA-MB 231 breast cancer cell line after 24 hours of treatment. Data presented as Mean

6.3.4 Cell culture studies

6.3.4.1 Cytotoxicity assay

The cytotoxic and antiproliferative effect of the prepared nanoparticles was assessed on MDA-MB-231 cells using the MTT assay. The cells were treated with various concentrations of free CBT, HA-OA/CS-OA NP, and HA-OA/CS-OA NPT for 24 h to determine their IC_{50} values. All the groups treated with either formulation or free drug induced significant concentration-dependent inhibition of the MDA-MB-231 cell line growth (**Figure 6.9**).

The free CBT-treated group exhibited an IC_{50} value of 3.708 ± 0.192 µg/ml after 24 hours of treatment. While the CBT-loaded nanoparticles HA-OA/CS-OA NP and HA-OA/CS-OA NPT showed an IC_{50} value of 2.111 ± 0.150 µg/ml and 1.061 ± 0.162 µg/ml respectively. The results indicate that CBT-loaded HA-OA/CS-OA NP and HA-OA/CS-OA NPT require only 57% and 28.5% of CBT dose respectively, to elicit the same cytotoxic response as free CBT. In other words, HA-OA/CS-OA NP exhibited a 1.75-fold reduction, while HA-OA/CS-OA NPT showed a 3.5-fold reduction in IC_{50} value in comparison to free CBT. These observations may be attributed to the inhibition of p-gp mediated drug efflux due to presence of TPGS-COOH, increased internalization of nanoparticles, and receptor-mediated endocytosis of cetuximab-conjugated HA-OA/CSOA NPT [247]. To confirm this, cellular uptake study was also conducted in MDA-MB-231 cells.

6.3.4.2 Cellular uptake study

Fluorescence microscopic images in **Figure 6.10** showed a higher cellular internalization potential of HA-OA/CS-OA NP and HA-OA/CS-OA NPT in comparison to free coumarin-6. This could be attributed to amphiphilic characters of the HA-OA and CS-OA conjugates rendering the overall structure of the nanoparticle deformable. Also, the

presence of TPGS-COOH in the particle structure improves cellular localization via P-gp inhibition. In addition, HA-OA/CS-OA NPT showed the highest cellular uptake in MDA-MB-231 cells, showing maximum emission of green fluorescence in the cytoplasmic region than other groups that may be attributed to cetuximab-directed uptake in MDA-MB-231 cells. The role of cetuximab in assisting targeted cellular internalization of nanoparticles was confirmed by blocking study, where diminished uptake was observed in groups pretreated with cetuximab. The pretreatment of Cetuximab allows competitive binding of the antibody to EGFR causing hindrance in receptor-mediated endocytosis of HA-OA/CS-OA NPT.

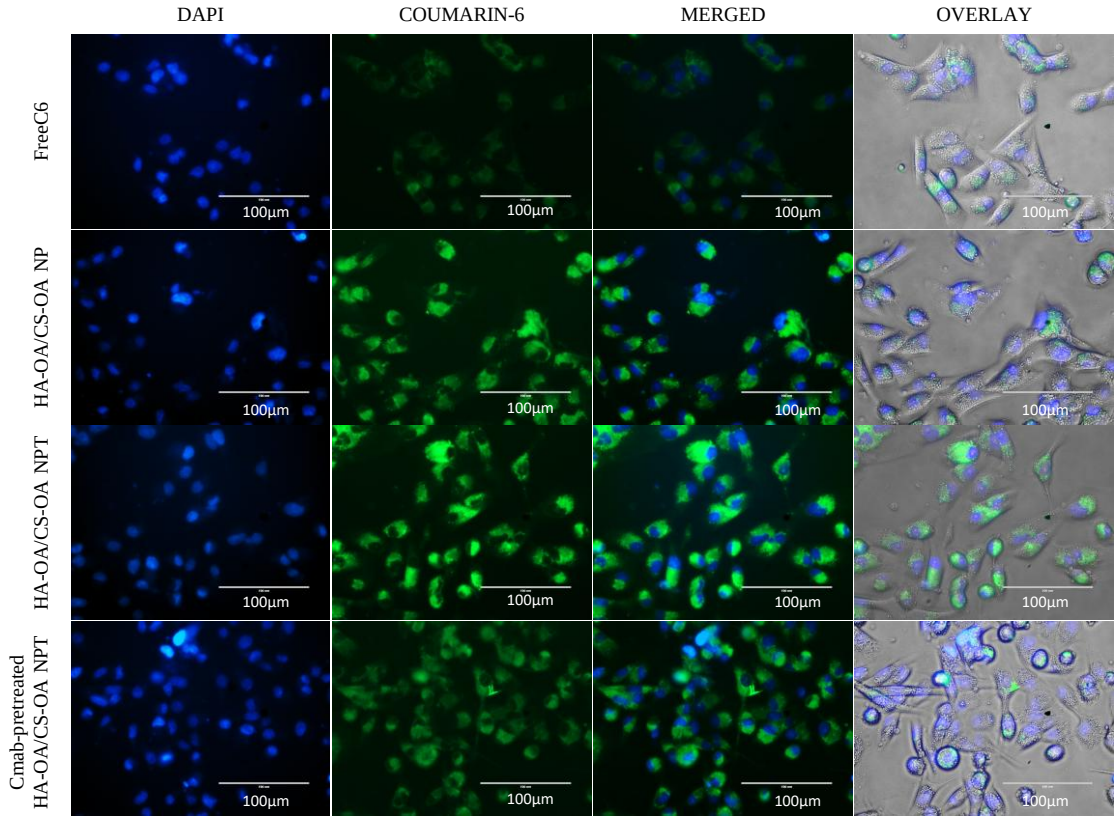

Figure 6.10 Fluorescence microscopy images of MDA-MB-231 cells after 6 hours incubation with free C6 and various HA-OA/CS-OA NP, HA-OA/CS-OA NPT, and Cmab-pretreated HA-OA/CS-OA NPT. GFP channel showing a higher level of green fluorescence in HA-OA/CS-OA NP and HA-OA/CS-OA NPT treated cells as compared to

freeC6. Cmab-pretreated HA-OA/CS-OA NPT treatment showed diminished fluorescence than HA-OA/CS-OA NPT treatment. Images were captured through an inverted fluorescence microscope at 400X magnification and 100 µm scale bar.

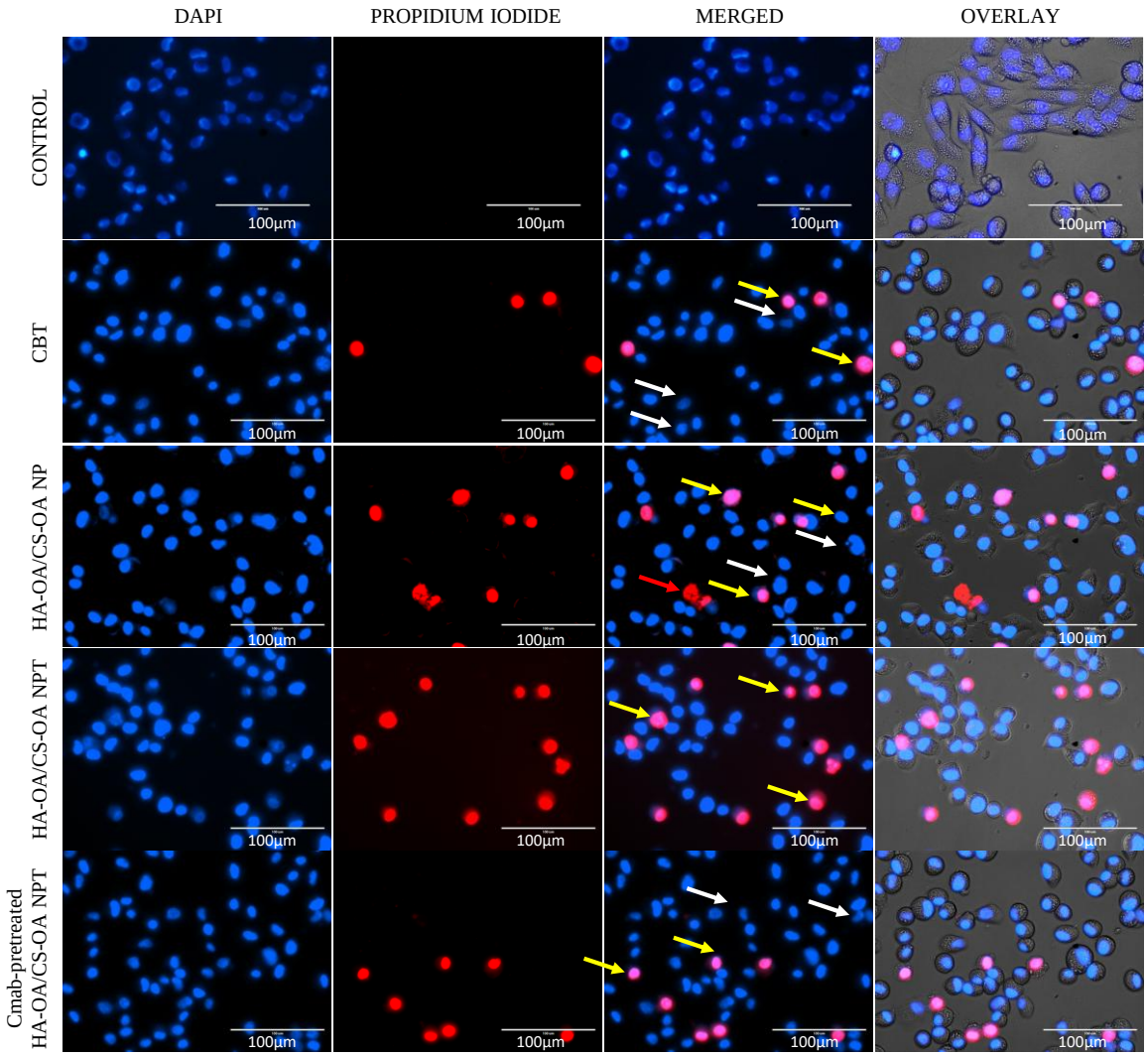

Figure 6.11 Combined microscopic images of Hoechst33342 / PI-stained MDA-MB-231 cells after 24 hours of treatment with free CBT, HA-OA/CS-OA NP, HA-OA/CS-OA NPT, and Cmab-pretreated HA-OA/CS-OA NPT. The white, yellow, and red arrows represent early apoptotic, late apoptotic, and necrotic cells. Cells emitting blue fluorescence (DAPI channel) are Hoechst positive while those with red fluorescence (PI channel) are PI positive.

6.3.4.3 Microscopic assessment of nuclear morphology

The apoptotic cells exhibit chromatin condensation in the nucleus and loss of plasma membrane integrity. These changes can be observed by staining the treated cells with the Hoechst33342/PI dye combination. Hoechst33342 dye stains the chromatin, which, due to condensation, appears brighter in apoptotic cells. While PI, a DNA-binding dye, only permeates into dead cells due to loss of membrane integrity. After treatment with free CBT, HA-OA/CS NP, and HA-OA/CS NPT the nucleus exhibited blue fluorescent with brighter intensity in comparison to the control group, indicating the presence of apoptotic and dead cells **Figure 6.11**.

The number of PI-stained cells was found to be highest in the HA-OA/CS-OA NPT treated group, followed by HA-OA/CS-OA NP and CBT, indicating their order of reducing cytotoxic effect. While the control group showed low-intensity blue fluorescence and negligible signals of red fluorescence of PI indicating live cells. Furthermore, the cetuximab pretreated cell exhibited a reduction in apoptosis that conforms with the observations from earlier studies, confirming the role of receptor in cellular internalization of the targeted nanoparticle.

6.3.4.4 Mitochondrial membrane potential

CBT, upon exposure, induces a decline in mitochondrial membrane potential. The JC-1 staining is an established method to assess this change in mitochondrial potential. In principle, the J-aggregates (red fluorescent signals) are primarily formed on mitochondria with normal membrane potential while a higher number of J-monomers (green fluorescent signals) can be seen as the membrane potential declines. The control group elicited red signals, indicating no decline in mitochondrial membrane potential. While CBT and HA-OA/CS-OA NP-treated cells exhibited predominantly red fluorescence, a marked increase

in green fluorescence can be seen in HA-OA/CS-OA NP-treated cells in comparison to free CBT-treated cells **(Figure 6.12)**.

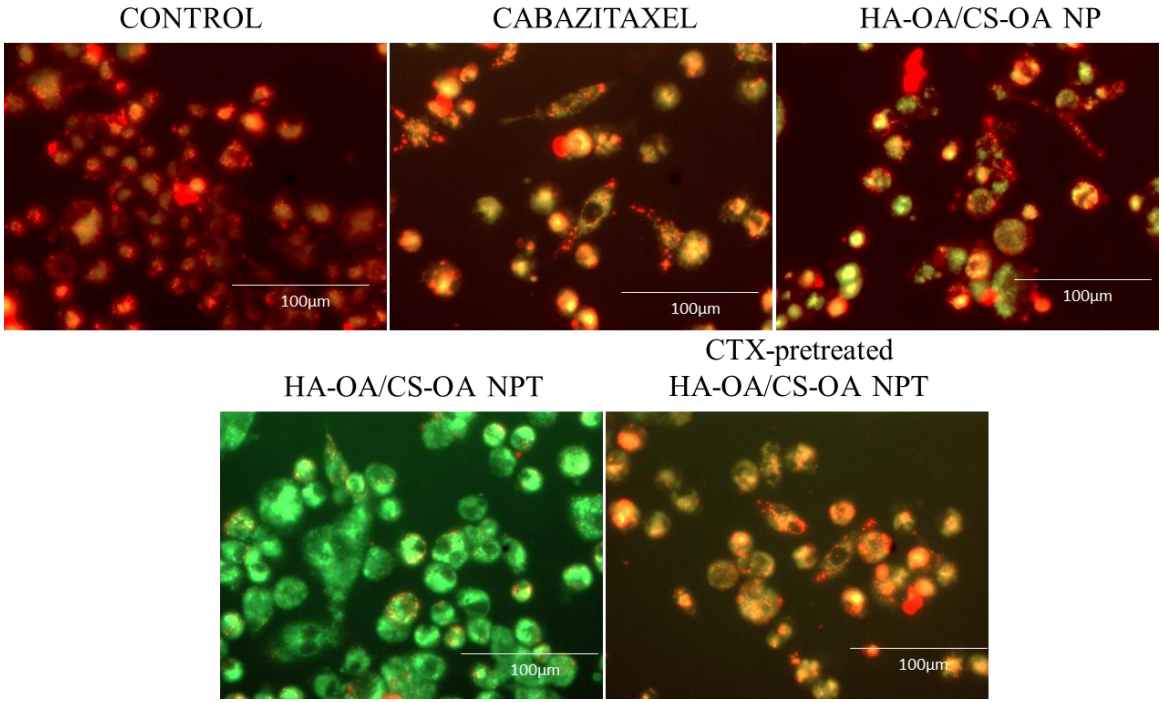

Figure 6.12 The impact of free-CBT, HA-OA/CS-OA NP, and HA-OA/CS-OA NPT treatment on the mitochondrial membrane potential of MDA-MB-231 cells was assessed using JC-1 staining after 24 hours of treatment. The increase in green fluorescence emission indicates a decrease in mitochondrial membrane potential upon treatment, with the highest decline seen in HA-OA/CS-OA NPT-treated cells. Red fluorescence indicates normal potential. Cells were examined using an inverted fluorescence microscope at 400X magnification.

However, HA-OA/CS-OA NPT treatment showed a rapid decline in mitochondrial membrane potential that led to predominantly green signals. This rapid decline and superior cytotoxic effect may be attributed to the enhance cellular internalization of HA-OA/CS-OA NPT as the green signals again diminished upon pretreatment with Cetuximab.

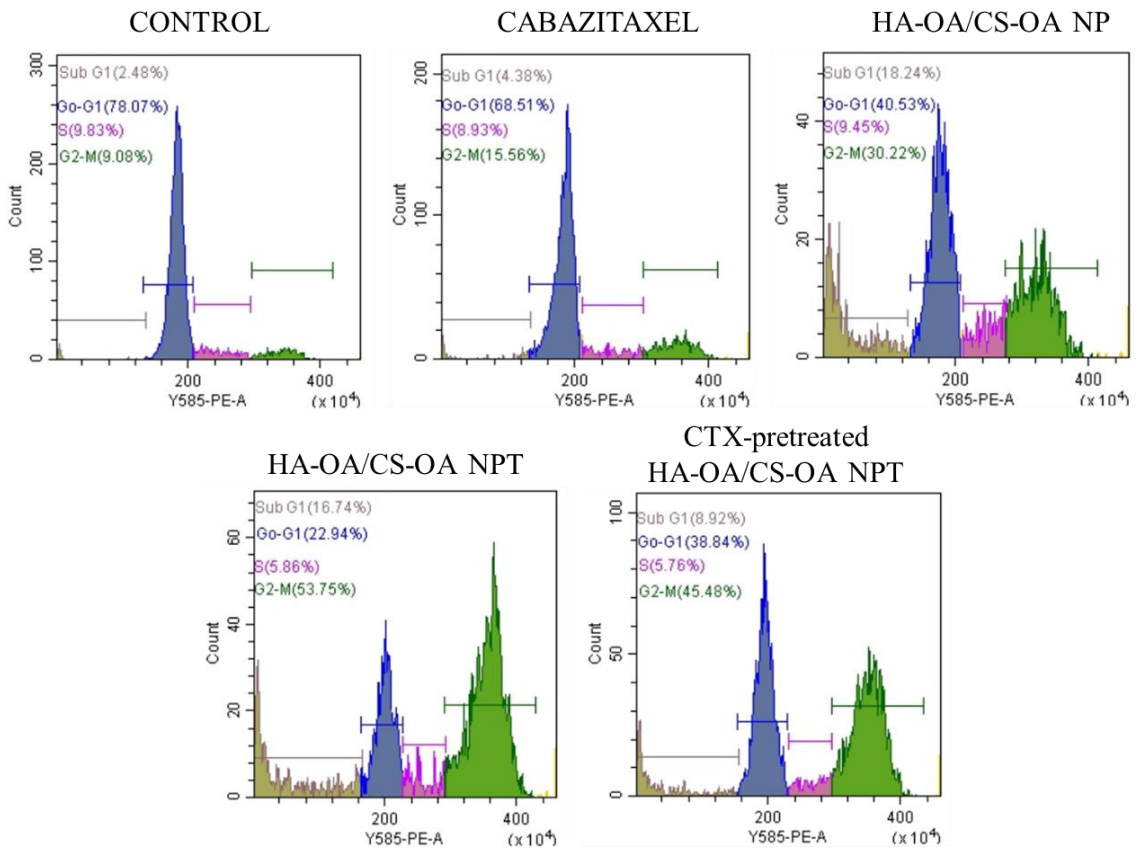

Figure 6.13 Plot denotes the flow cytometric data of free-CBT, HA-OA/CS-OA NP, and HA-OA/CS-OA NPT treated MDA-MB-231 cells. PI staining was done to determine the percentage of cells in different phases of the cell cycle. HA-OA/CS-OA NPT treated cells showed a significant (***$p < 0.001$) increase in cell population in the G2-M phase in comparison to the control. A significant difference between various treatment groups was also observed. Free-CBT and HA-OA/CS-OA NP (***$p < 0.001$), free-CBT and HA-OA/CS-OA NPT (***$p < 0.001$), and HA-OA/CS-OA NP and HA-OA/CS-OA NPT (**$p < 0.01$) was observed.

6.3.4.5 Quantification of DNA content through cell cycle analysis

CBT induces cell cycle arrest at the G2/M phase. To evaluate whether the anti-proliferative effect of HA-OA/CS-OA NP and HA-OA/CS-OA NPT is due to the cell cycle arrest caused by CBT loaded in the formulation cell cycle analysis study was performed. The cells were treated with CBT, HA-OA/CS-OA NP and HA-OA/CS-OA NPT at

concentrations equivalent to the IC_{50} value of HA-OA/CS-OA NPT. The DNA binding dye PI used in the study stains the DNA stoichiometrically, allowing differentiation in various phases of the cell cycle. The data indicate that there is a significant increase in the population of cells in the G2/M phase of the cell cycle treated with HA-OA/CS-OA NP (~2-fold) and HA-OA/CS-OA NPT (~3.5-fold) when compared to the free CBT treated (15.56%) **Figure 6.13**. The superior cell cycle arrest caused by the nanoparticles and a significant decline in cell cycle arrest in cetuximab pretreated cell (53.75% to 45.48%) indicate that the nanoparticles facilitate higher intracellular accumulation of CBT via. receptor-mediated endocytosis resulting in improved cytotoxic and anti-proliferative effect.

6.3.5 Fabrication and evaluation of dissolving MN

The MN were prepared using a polymeric blend of HA, PVA and PVP while its backing consists of only PVA matrix. **Figure 6.14** showed the photograph and SEM image of fabricated MN in horizontal and vertical position.

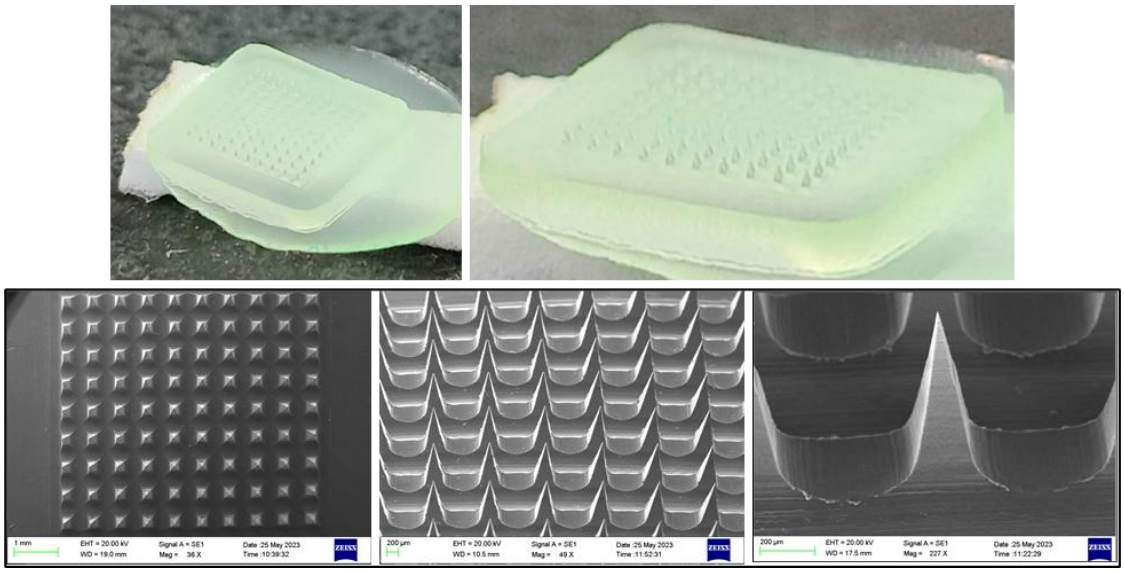

Figure 6.14 Photograph and Scanning Electron Microscopy (SEM) images of HA-OA/CS-OA NPT MN

The microscopy images revealed pyramidal shaped MN with an average height of 561.18 ± 5.34 µm. The microneedles had a smooth surface with no observable cracks or fractures. HA-OA/CS-OA NPT were dispersed in the polymeric blend and molded into microneedles for fabrication of targeted nanoparticles loaded microneedles. HA-OA/CS-OA NPT-MN were observed to be of height 546.25± 3.92 µm, indicating that the microneedles can potentially permeate through rat skin to reach the tumor tissue [251]. The amount of drug-loaded nanoparticles in the microneedles array and base layer was equivalent to approximately 250µg of CBT. However, the combined volume of all the 100 microneedles in the array is approximately 0.00073 ml, so most of the drug is loaded in the base layer.

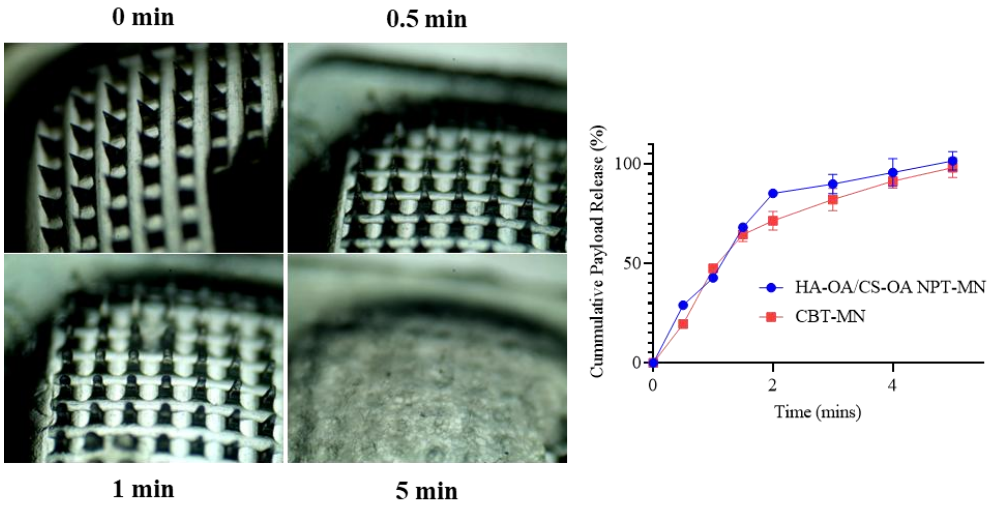

Figure 6.15 Microscopic images of HA-OA/CS-OA NPT MN after exposure to PBS pH 7.4 and dissolution of microneedles in PBS pH 7.4 (calculated in terms of percentage therapeutic payload release w.r.t. time).

6.3.5.1 Solid-state characterization of dissolving MN

The spectroscopic analysis including FTIR, XRD and DSC was also conducted for prepared MN (**Figure 6.7 & Figure 6.8**). MN 3185 cm^{-1} (-OH stretching of HA/PVP/PVA), 2799 cm^{-1} (-CH stretching of HA, PVP, PVA), 1512 cm^{-1} (C=O stretching

of HA and PVP), 1272 cm^{-1} (C–N stretch of PVP and HA), 1222 cm^{-1} (-CH bending of PVP), 1142 cm^{-1} (C-O- stretch of PVA), and 884 cm^{-1} (C-C breathing of PVP/PVA) [235,252,253]. The diffraction pattern of MN showed peaks at 2θ value 13.307, 15.979, and 24.677 corresponding to PVA. The thermogram of MN exhibited endothermic peaks at 185℃ and 214℃ attributed to HA/PVP/PVA blend used for fabrication of microneedles [254].

6.3.5.2 In vitro dissolution study

The microneedles dissolution study was conducted to assess the time required by microneedle to dissolve after exposure to moisture/aqueous medium and release the payload. Microscopic images in **Figure 6.15**, shows the swelling and dissolution of microneedles with respect to time. Within first 2 minutes the needle-array has completely dissolved and release the payload in the media. The payload here refers to the loaded CBT in case of CBT-MN and CBT loaded HA-OA/CS-OA NPT in case of HA-OA/CS-OA NPT-MN. The addition of methanol in the aliquots collected from the wells and sonication for 30 minutes allows the dissolution of the drug entrapped in HA-OA/CS-OA NPT. The study was performed to assess the dissolution of the microneedle array and not the drug release. CBT-MN started to dissolve instantaneously on coming contact with media (as seen in **Figure 6.15**), releasing about 19.53 ± 0.69 % payload within 0.5 min, 71.44 ± 4.69 % in 2 min and almost complete DMN dissolution in about 5 min to provide 98.10 ± 4.96 % payload release. In comparison to CBT-MN, HA-OA/CS-OA NPT-MN showed slightly faster payload release of 28.98 ± 0.54 % in 0.5 min and 85.24 ± 1.35 % in 2 min. The drug release and drug permeation across skin was later evaluated using Franz diffusion cell and rat skin.

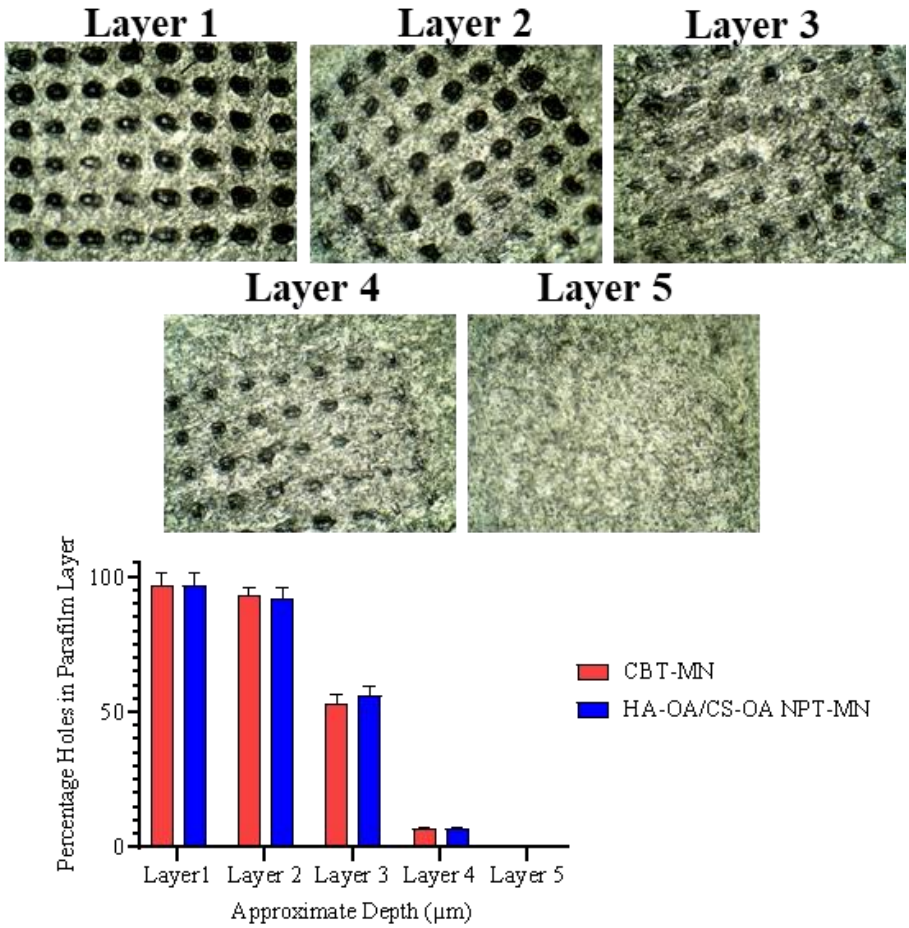

Figure 6.16 Images of parafilm layers after insertion of HA-OA/CS-OA NPT MN. The histogram represents the percentage of holes created in each layer of parafilm by microneedles after manual insertion

6.3.5.3 In vitro penetration assay using Parafilm®

The MN capability of skin insertion was investigated *in vitro* using Parafilm® method. The insertion ability was determined in terms of percentage holes created in each layer of parafilm (**Figure 6.16)**. MN was observed to efficiently pierce the 3 layers of parafilm. The percentage holes created by microneedle array up to 260 µm (2 layers of parafilm) was > 95%. However, ~70% holes were created in the third parafilm layer (390 µm depth). The tips of microneedle array were able to reach even the fourth layer of parafilm without creating holes. The result indicate that the microneedle array has an average penetration

depth of 340-360 µm i.e. approximately 65% of MN height. Similar results of penetration depth in case dissolving microneedles have been reported [255].

6.3.5.4 Ex vivo skin penetration assay

The MN skin insertion ability was also checked *ex vivo* using rat skin. The MN applied to skin (thickness 450 µm) penetrated in the skin on applying manual pressure. The microscopic observations revealed the formation of microchannels created due to MN insertion as shown in **Figure 6.17(A)** [256]. The *ex vivo* skin insertion result was consistent with the results obtained from *in vitro* parafilm insertion study.

To study the role of microneedles in drug permeation and retention in or across skin, *ex vivo* skin permeation study was conducted **(Figure 6.17(B)**.

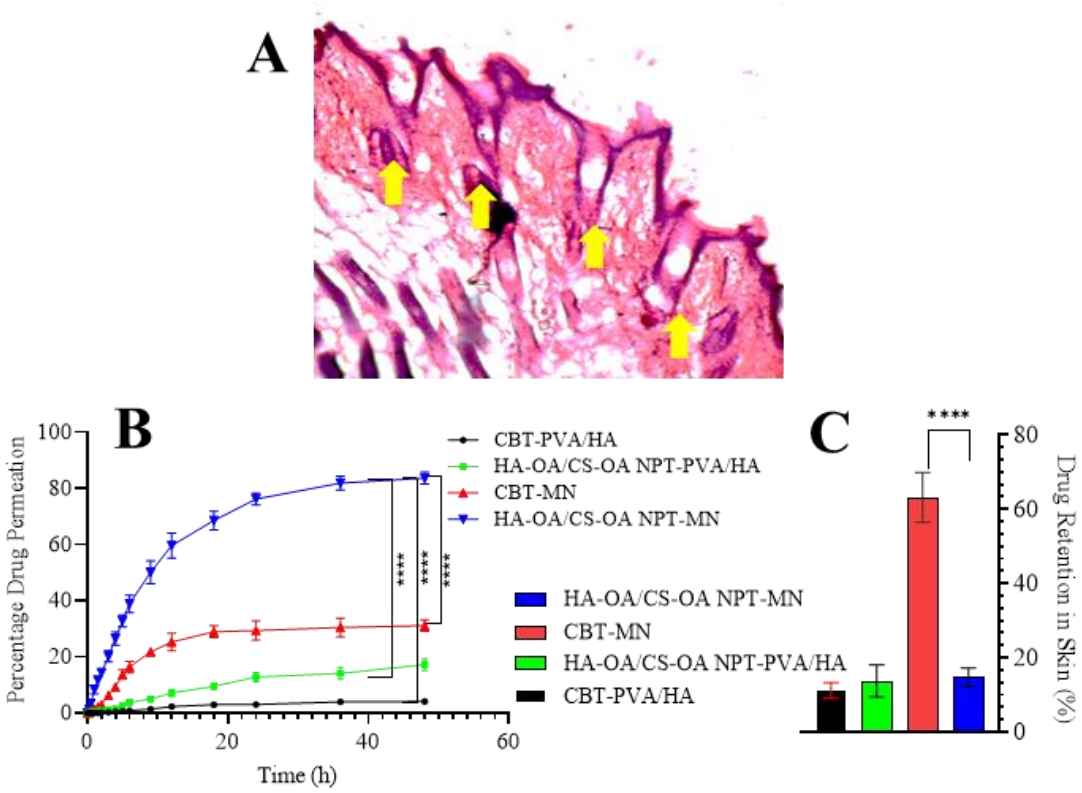

Figure 6.17 (**A**) Microscopic image of rat skin after HA-OA/CS-OA NPT MN insertion. (**B**) Graph representing ex vivo drug permeation across rat skin determined using a Franz diffusion cell. HA-OA/CS-OA NPT-MN showed significant improvement in drug

permeation in comparison to CBT-MN and HA-OA/CS-OA NPT loaded PVA/HA blend (****p value < 0.001) **(C)** Representation of percentage drug retention in skin after 48 hours of drug permeation study.

Pure drug and nanoparticle-loaded HA/PVA/PVP blends were used for comparison with drug and nanoparticles loaded microneedles. CBT-PVA/HA showed poor drug permeation of only 4.11±0.39%, while HA-OA/CS-OA NPT-PVA/HA exhibited permeation of about 17.23±2.13% in 48h. The poor permeation was attributed to low solubility and permeability potential of pure drug that showed marginal increase in case of HA-OA/CS-OA NPT loaded HA/PVA/PVP blend. Compared to CBT-PVA/HA and HA-OA/CS-OA NPT-PVA/HA, CBT-MN significantly (**p<0.01) increased the drug permeation to about 31.12±2.1% probably due to formation of microchannels created by microneedle array penetration in the skin facilitating deeper and faster permeation of payload [255].

However, HA-OA/CS-OA NPT-MN exhibited highest permeation of about 83.62±2.09% suggesting role of microchannels created by microneedles complimented with superior mobility of the nanoparticles into skin [257]. In addition, the retention of drug in skin was maximum with CBT-MN followed by HA-OA/CS-OA NPT-MN, HA-OA/CS-OA NPT-PVA/HA, and CBT-PVA/HA **(Figure 6.17(C)**. The retention of drug could be due to depot formation of released payload at the site [257,258]. The highest retention of pure drug in MN could be due to poor solubility and permeability of CBT. The HA-OA/CS-OA NPT-MN had highest permeation due to its superior mobility and deformability that allo through the skin and reach the acceptor compartment.

6.3.6 In vivo studies

6.3.6.1 Tumor regression analysis

In vivo tumor efficacy of CBT (i.v.), CBT-MN and HA-OA/CS-OA NPT-MN was determined and comparative tumor volume are shown in **Figure 6.18**. Tumor volume

found to change with time during the study. HA-OA/CS-OA NPT-MN and CBT-MN treated group had significantly ($p<0.0001$) higher tumor inhibition compared to CBT (i.v.). HA-OA/CS-OA NPT-MN treated groups showed 5.24- and 27.5-folds reduction in tumor volume than the groups treated with CBT-MN and CBT (i.v.), at day 14. Also, the tumor volume in the HA-OA/CS-OA NPT-MN treated group showed approximately 68-folds reduction in tumor volume over the period of 14-day treatment. Similarly, CBT-MN treated group exhibited a 4.7-folds decline in tumor volume during the same period. However, a 10 percent increase in tumor volume was observed in CBT (i.v.) treated group. The higher tumor inhibition efficacy of HA-OA/CS-OA NPT-MN was due to combined effect of improved permeation to the tumor site, regioselective delivery of the nanoparticles, and their receptor-mediated intracellular accumulation.

The assessment of body weight of Normal SD rats, untreated tumor bearing rats, CBT (i.v.), CBT-MN and HA-OA/CS-OA NPT-MN was also carried out (**Figure 6.19(A))**. The change in body weight of the formulation treated groups was compared to Normal SD rats receiving no treatment. There was no significant change in body weight if animals treated with HA-OA/CS-OA NPT-MN ($p >0.9999$) and CBT-MN ($p = 0.4263$) in comparison to healthy untreated SD rats. Whereas, the body weight was significantly different for untreated tumor bearing rats (0.0035), and CBT (i.v.) (<0.0001). The increase in the body weight of tumor bearing untreated rats may be attributed to the rapidly increasing tumor volume. While, the decrease in body weight of CBT (i.v.) treated group indicated that the non-targeted and non-selective distribution of CBT has resulted in systemic toxicity.

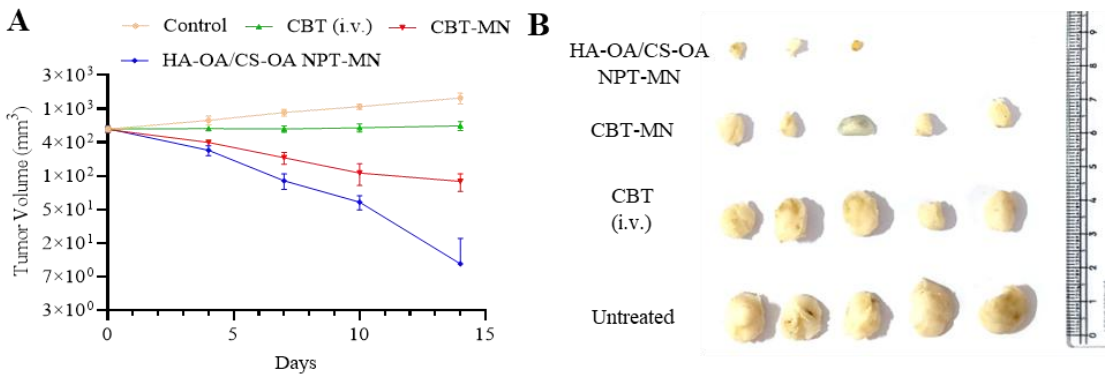

Figure 6.18 (A) Tumor regression analysis in Tumor-bearing female SD rats; Tumor volume of control, CBT (i.v.), CBT-MN, and HA-OA/CS-OA NPT-MN treated groups during a 14-day treatment period. **(B)** Image of tumors collected from treatment groups after 14 days of treatment.

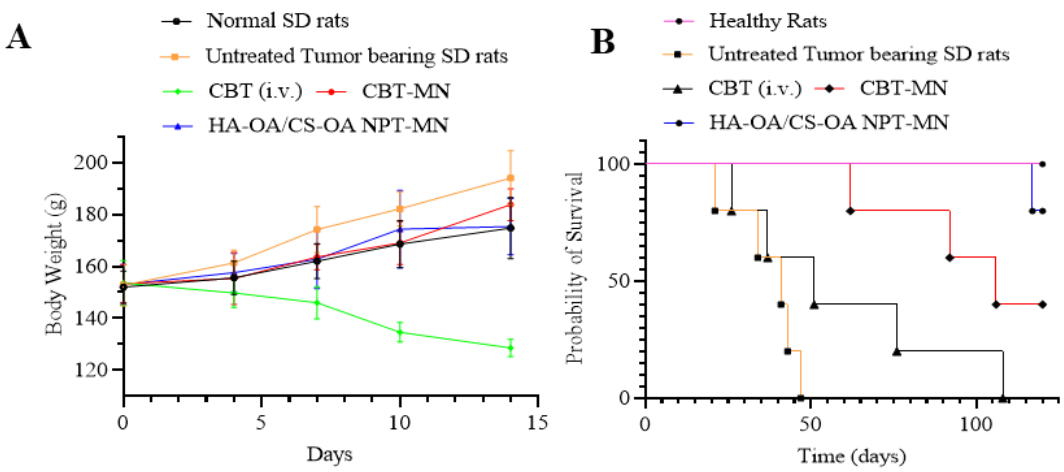

Figure 6.19 (A) Body weight of healthy female SD rats and tumor-bearing female SD rats receiving CBT (i.v.), CBT-MN, and HA-OA/CS-OA NPT-MN treatment for a 14-day treatment regimen. **(B)** The Kaplan-Meier survival probability plot (120 days) of Healthy and tumor-bearing female SD rats treated with CBT (i.v.), CBT-MN, and HA-OA/CS-OA NPT-MN treated groups.

6.3.6.2 Survival analysis

The survival rate of HA-OA/CS-OA NPT-MN was also significantly higher compared to untreated tumor bearing rats, CBT (i.v.), and CBT-MN. The median survival rate for untreated tumor bearing rats, CBT (i.v.), CBT-MN and HA-OA/CS-OA NPT-MN was 41, 51, 106 and >120 days, respectively (**Figure 6.19(B)**). HA-OA/CS-OA NPT-MN treated group showed higher survival rate attributed to its low toxicity and high efficacy due to targeted drug delivery.

6.3.6.3 Histological assessment of tumor tissue

In histological analysis of H&E stained tissue, as shown in **Figure 6.20**, the control group showed normal cell pattern with regular shape and spherical/spindle shaped large blue nucleus [233]. While tumor induced model (untreated tumor, day 0) showed well defined cancer cells mass (red arrow), high nucleation and signs of high mucin secretion (yellow arrow). The untreated tumor showed fully developed cancer with highly nucleated cancer mass. CBT (i.v.) treated group found to control the tumor growth, although had signs of cancer cells and mucin secretion. CBT-MN treated group had lower cell density, and signs of cell shrinkage. HA-OA/CS-OA NPT-MN found to disappear the cancer cells and necrotic areas within the sections appeared. The appearance of spindle shaped nuclei, a condensed nucleoplasm, and regular cell density was also observed with HA-OA/CS-OA NPT-MN [233,235].

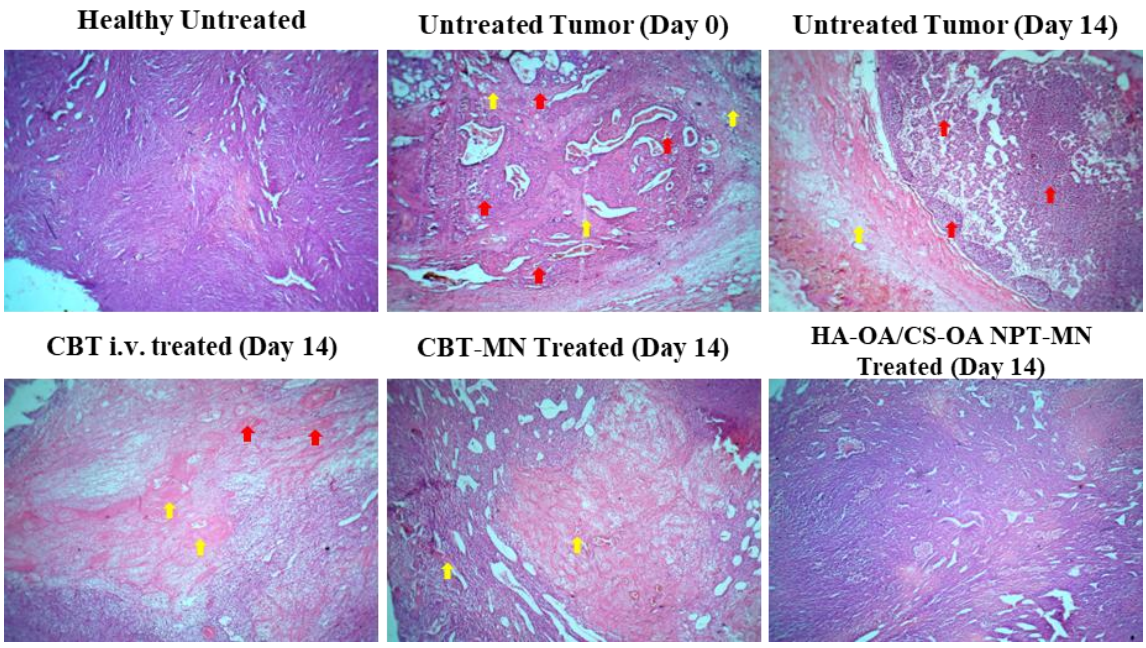

Figure 6.20 Histological images of H&E stained healthy/tumor tissues before and after 14-day treatment with CBT (i.v.), CBT-MN and HA-OA/CS-OA NPT-MN.

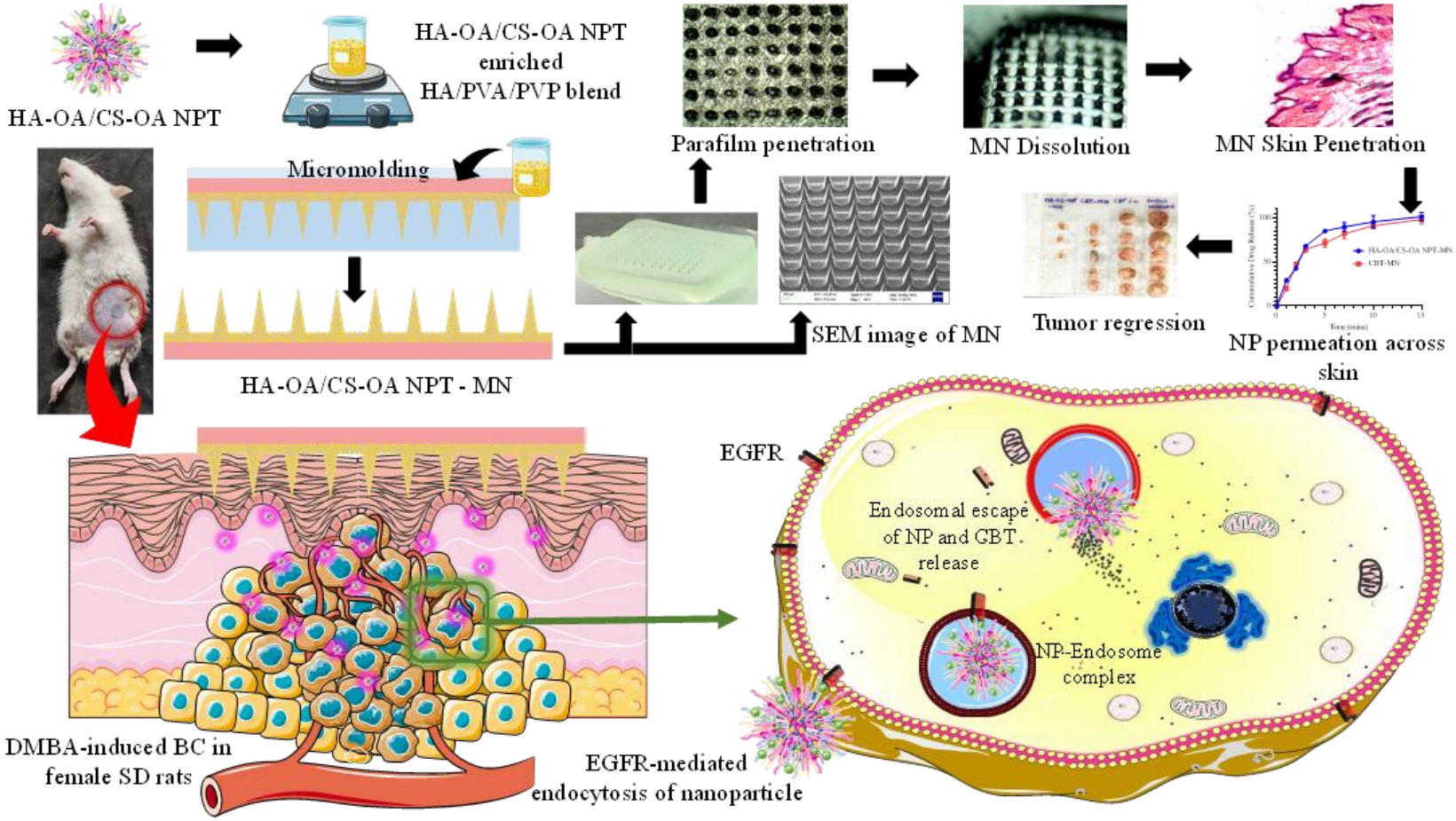

Figure 6.21 Graphical Abstract of Objective 3